Flow Physics and Heat Transfer for Jets in Crossflow-Applications in Gas Turbine Cooling

Sumanta Acharya[1], Prasad Kalghatgi[2] & Hessam Babaee[2]
Ring Companies Endowed Chair & Dept. Chair
Univ. of Memphis, TN

[2]Turbine Innovation & Energy Research (TIER) Center
Louisiana State University
Baton Rouge, LA
[1]Professor, [2]Doctoral Students

Sponsor: AFOSR, DOE-CPERC,
Computing Platforms: LSU-HPC, LONI, XSEDE

Gas Turbines: Applications

- Power Generation &
- Propulsion

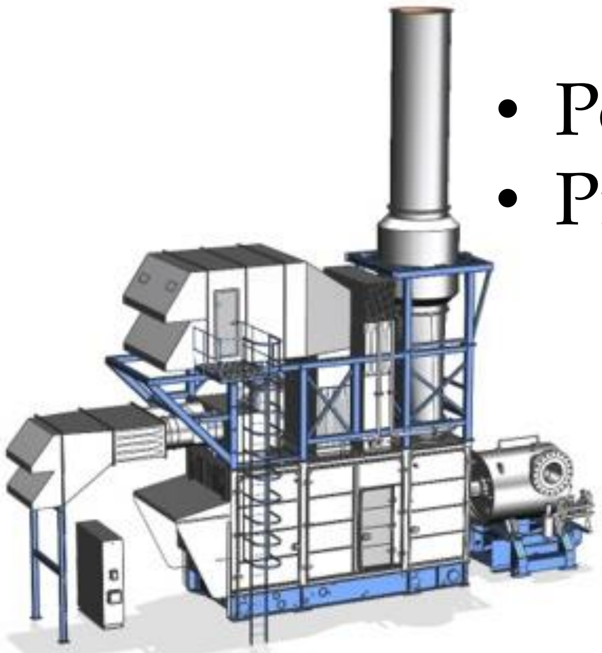

www.siemens.com

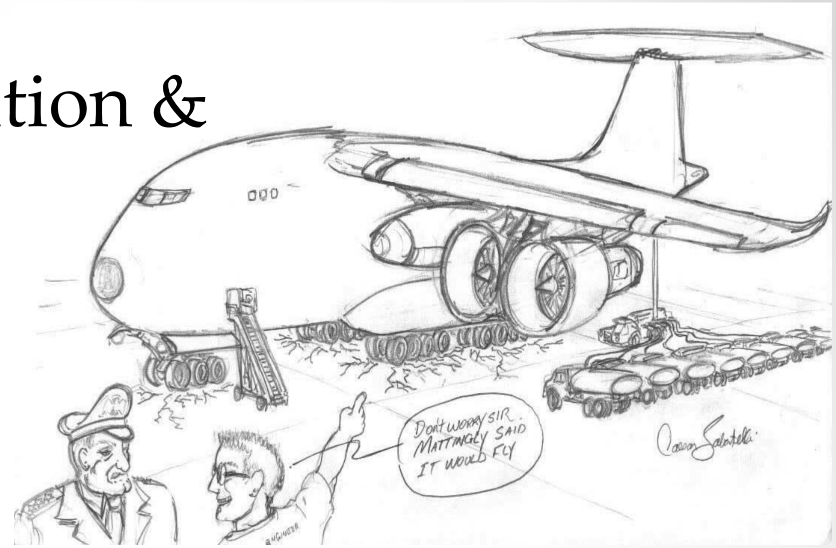

http://www.aircraftenginedesign.com

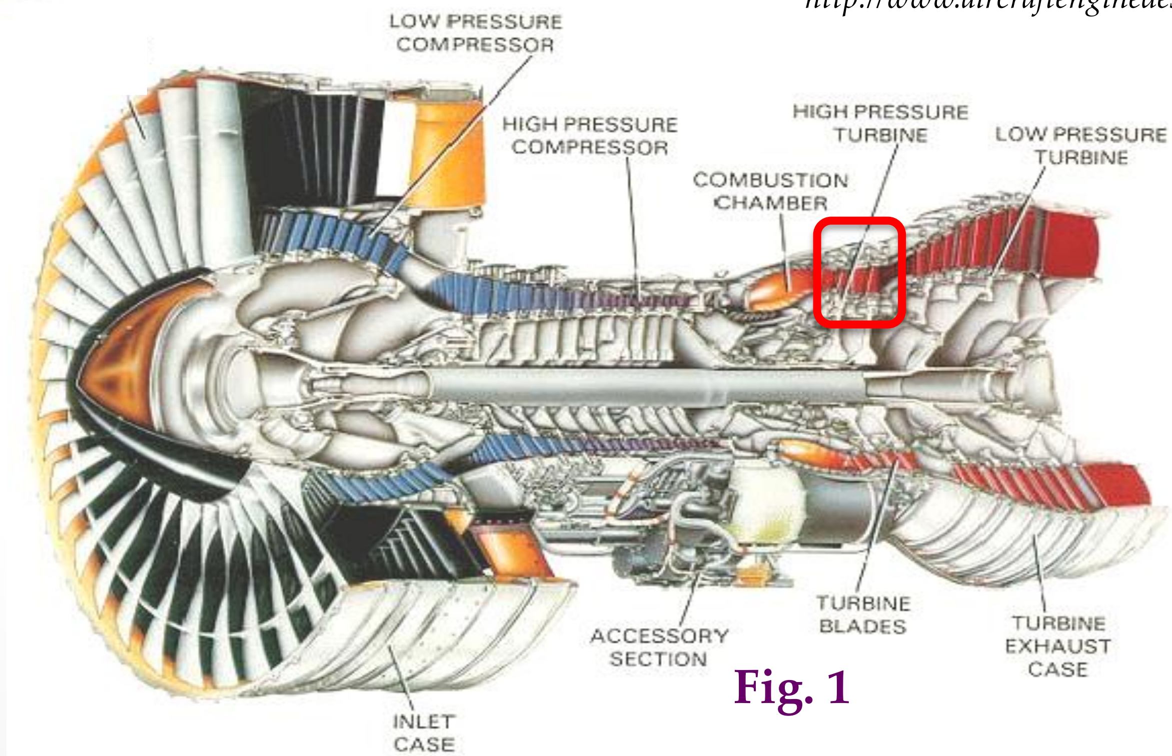

Fig. 1

Introduction

Because Turbine Inlet Temperatures exceed material limits, they have to be actively cooled to prevent blade/vane failure.

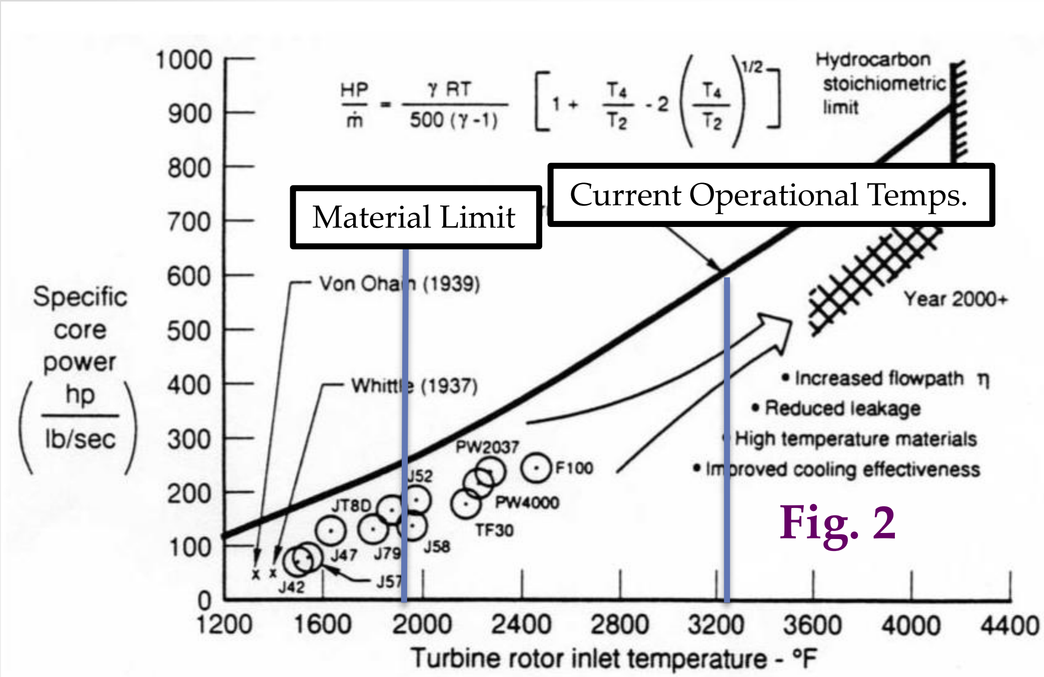

Fig. 2

Trend in Turbine inlet temperature *(Sautner AGARD 1992).*

Fig. 3

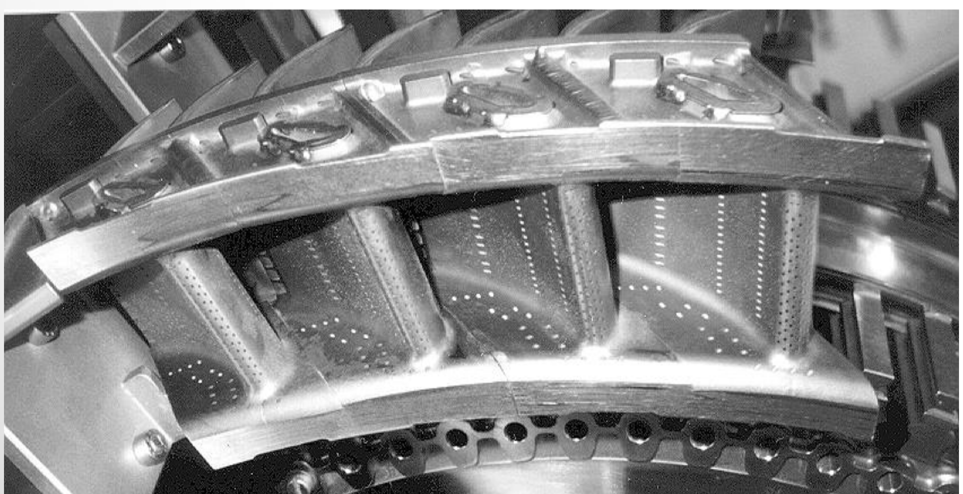

Fig. 4a Friedrichs, 1997

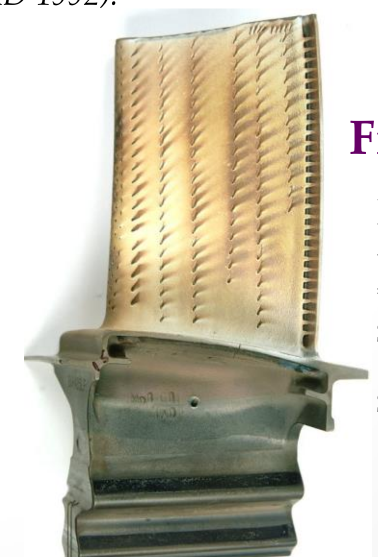

Fig. 4b

Heavily film cooled gas turbine blade

*Ronald Bunker - Turbine 09 Symposium on Heat Transfer in Gas Turbine System - 2009

Advanced Materials Coatings, Guo & Acharya, NASA

Actively Cooled Airfoil

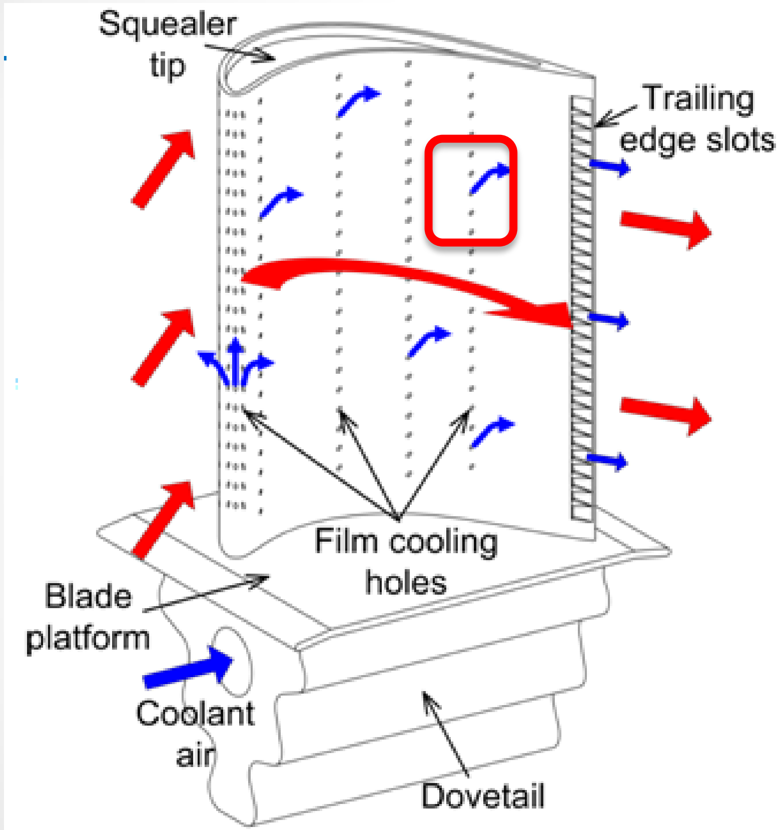

Conceptual view of blade external cooling

from Liu, Siemens

Fig. 5

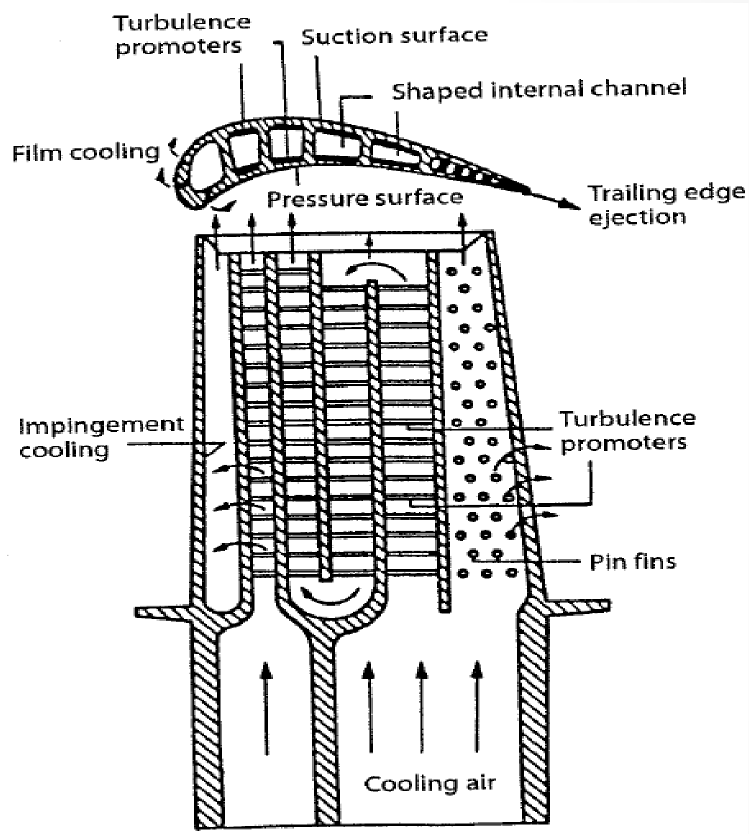

Conceptual view of blade internal cooling

(from Han, Texas A & M)

Fig. 6

Outline

- Introduction
  - Motivation
  - Problem Setup; Numerics; V & V
- Film Cooling Physics
  - *J. Turbomachinery, 2013*
- Film Cooling Geometry
  - *ASME Turbo Expo 2014, J. Turbomachinery 2015*
- Blowing Ratio Uncertainty-Quantification
  - *J. Heat Transfer 2013*
- Conclusions

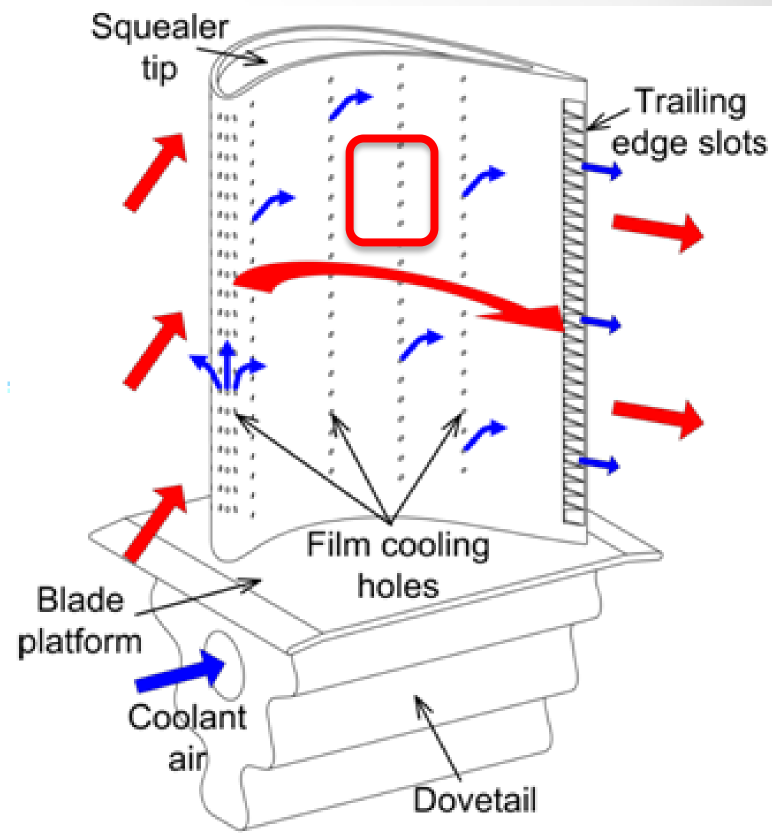

Conceptual view of blade external cooling

Film Cooling Jet: Expected Flow Structures

- Kidney pair (or Counter-Rotating-Vortex-Pair) - CVP
- Horse-shoe vortex
- Wall vortices
- Wake vortices
- Shear-layer vortices
- Counter Rotating Vortex Pair (CRVP or CVP)-Dominant Structure
- Dynamics of these structures control the near-field mixing

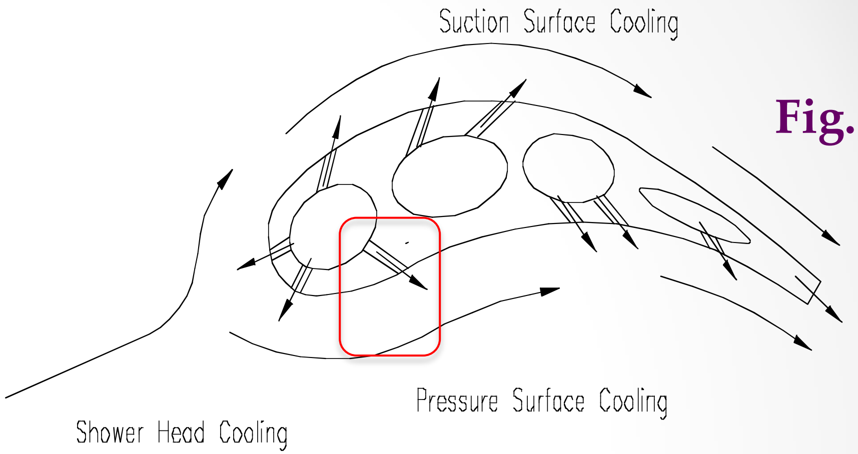

Fig. 7

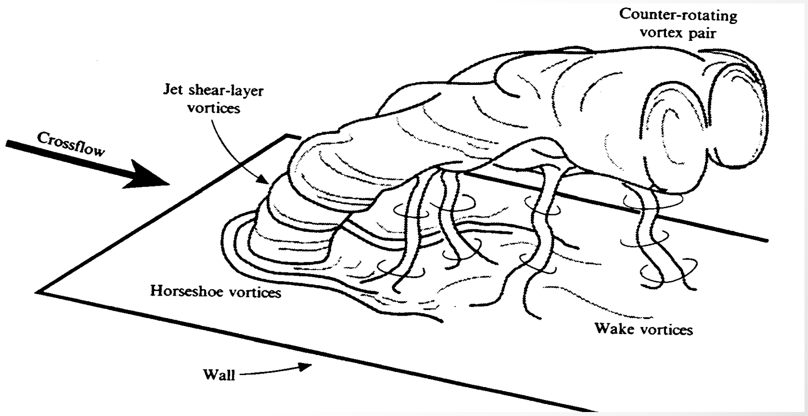

Fric and Roshko (1994)

Problem Definition

Film cooling of a flat surface with inclined cylindrical delivery tube fed with a plenum chamber

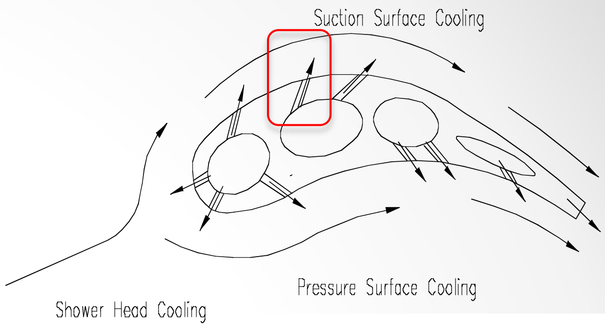

Geometry and Flow conditions

35^0 Inclined round jet (Diameter D = 12.7mm)

Short Delivery tube (l/D) = 1.75

Re_D = 16000 (Cross flow velocity 20m/s)

Density Ratio ρ_j/ρ_∞=2.0

Blowing Ratio $\rho_j V_j/\rho_\infty V_\infty$=1.0

Free stream fluid @ 300 K

Coolant fluid @ 150 K

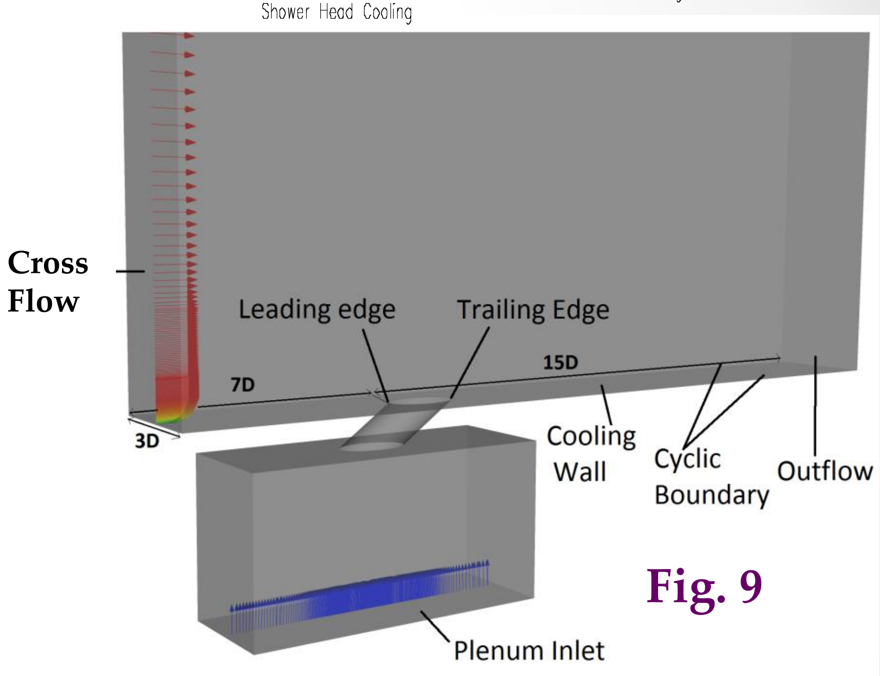

Fig. 9

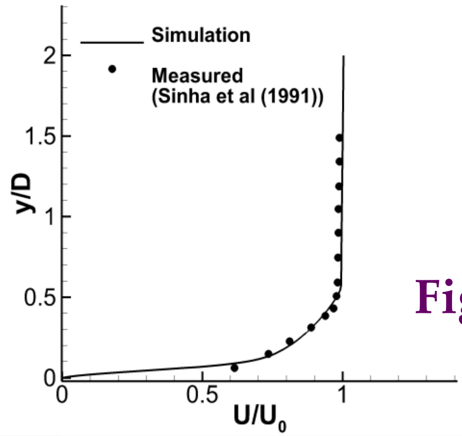

Fig. 10

Boundary layer profile @ x/D = -1.0

Numerical Tool and LES

- Transformed Continuity, Navier-Stokes and energy equations are solved

$$\frac{\partial}{\partial \xi}\left(\sqrt{g}U^{j}\right)=0$$

$$\frac{\partial}{\partial t}\left(\sqrt{g}\bar{u}_{j}\right)+\frac{\partial}{\partial \xi_{j}}\left(\sqrt{g}\bar{U}^{j}\bar{u}_{i}\right)=-\frac{\partial}{\partial \xi_{j}}\left(\sqrt{g}\,(a^{j})_{i}\,\bar{p}\right)+\frac{\partial}{\partial \xi_{j}}\left(\left(\frac{1}{\mathrm{Re}}+\frac{1}{\mathrm{Re}_{t}}\right)\sqrt{g}\,g^{jk}\frac{\partial \bar{u}_{i}}{\partial \xi_{k}}\right)$$

$$\frac{\partial}{\partial t}\left(\sqrt{g}\bar{q}\right)+\frac{\partial}{\partial x_{j}}\left(\sqrt{g}\bar{U}^{j}\bar{q}\right)=\frac{\partial}{\partial x_{j}}\left(\left(\frac{1}{\mathrm{Re}\,\mathrm{Pr}}+\frac{1}{\mathrm{Pr}_{t}\mathrm{Re}_{t}}\right)\sqrt{g}\,g^{jk}\frac{\partial \bar{q}_{i}}{\partial x_{k}}\right)$$

- Eddy viscosity evaluated using $1/\mathrm{Re}_{t}=C_{s}^{2}\sqrt{g}^{\,2/3}\,|\bar{S}|$
- Dynamic Smagorinsky model to evaluate coefficients

Flow solver

- Parallel Multi-block code in generalized curvilinear coordinate system
- 5th Order WENO scheme for convective terms
- Second order central difference for viscous terms
- Second order backward 3-point physical time differencing is used
- ILU solver for linear equations

Film Cooling Simulation-V & V

- Domain discretization – 680 blocks structured grids with 8 M Grid points based on a mesh independent study involving
- Physical time step $\Delta t u_{\infty} / D = 3.14 \times 10^{-3}$
- Transients were allowed to pass over (20k) ~5 flow through time (based on 15D downstream distance)
- Flow statistics collected over a 40k time steps (10 flow through time based on streamwise distance of 15D)

COOLING EFFECTIVENESS = NON DIMENSIONAL SURFACE TEMPERATURE

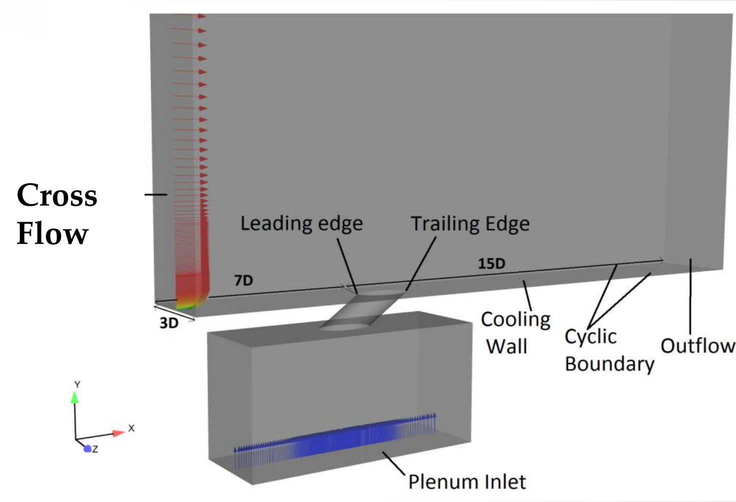

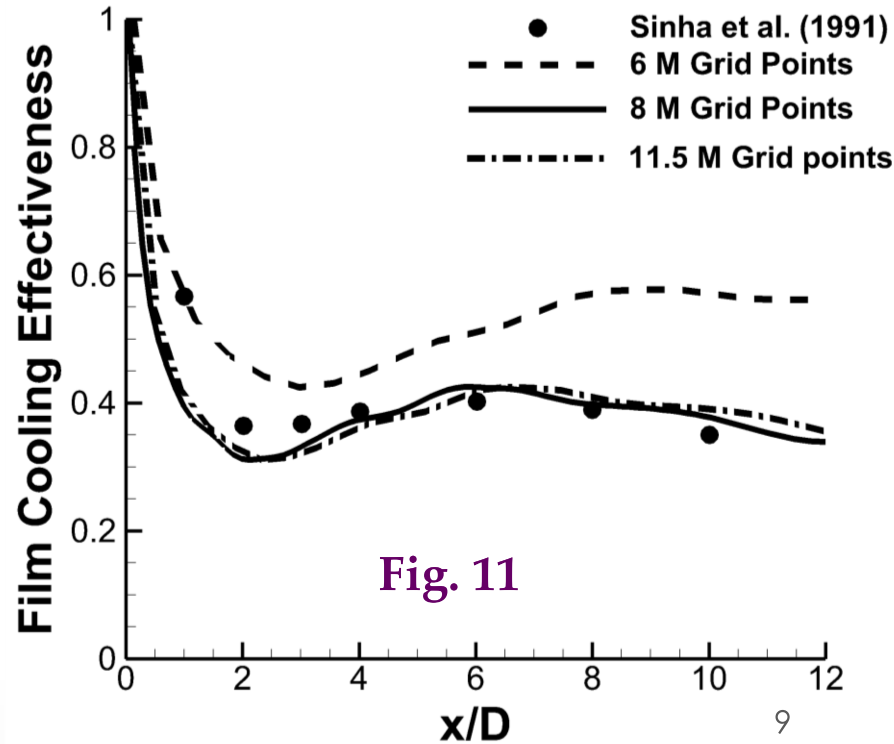

Fig. 11

Validation

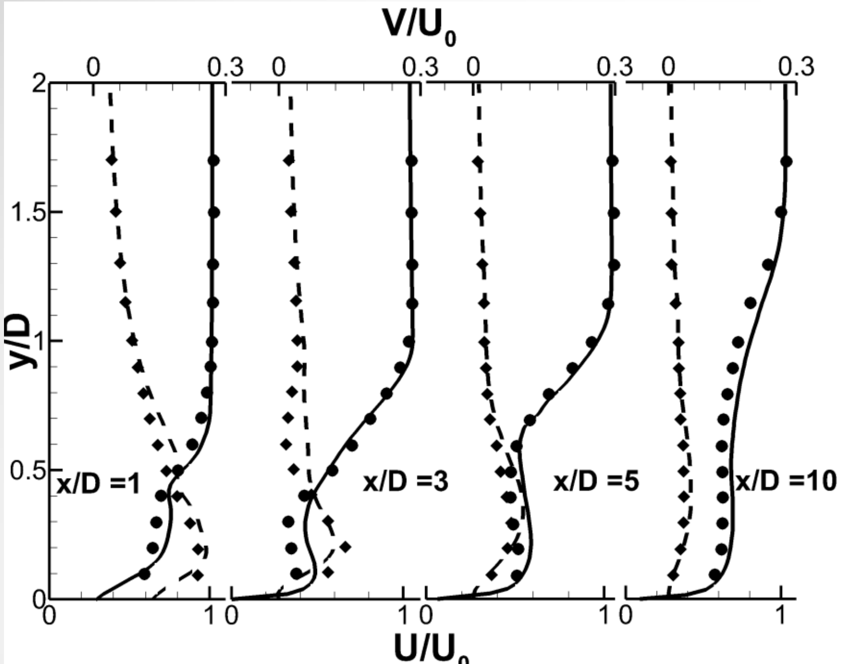

•U/U_0(exp), ◆V/U_0 (exp),– U/U_0, —V/U_0

Streamwise and wall normal velocity measurements

Fig. 12

Sinha, A.K., D.G. Bogard, and M.E. Crawford, *Film-Cooling Effectiveness Downstream of a Single Row of Holes With Variable Density Ratio*. Journal of Turbomachinery, 1991. 113: p. 442-449.

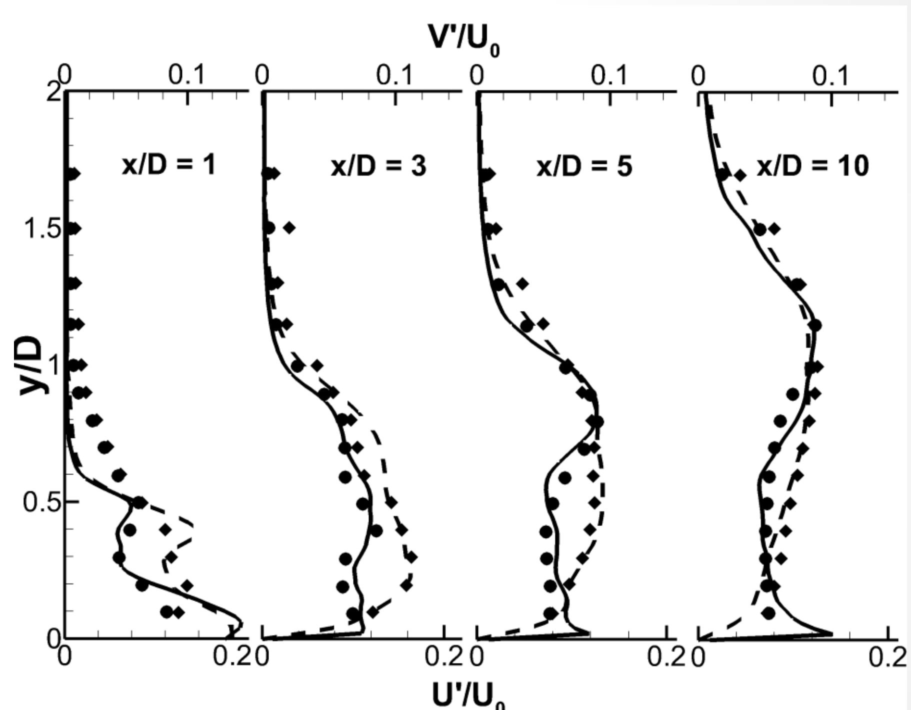

Fig. 13

•U'/U_0(exp), ◆V'/U_0 (exp),– U'/U_0, —V'/U_0

Streamwise and wall normal RMS velocity

Film cooling effectiveness

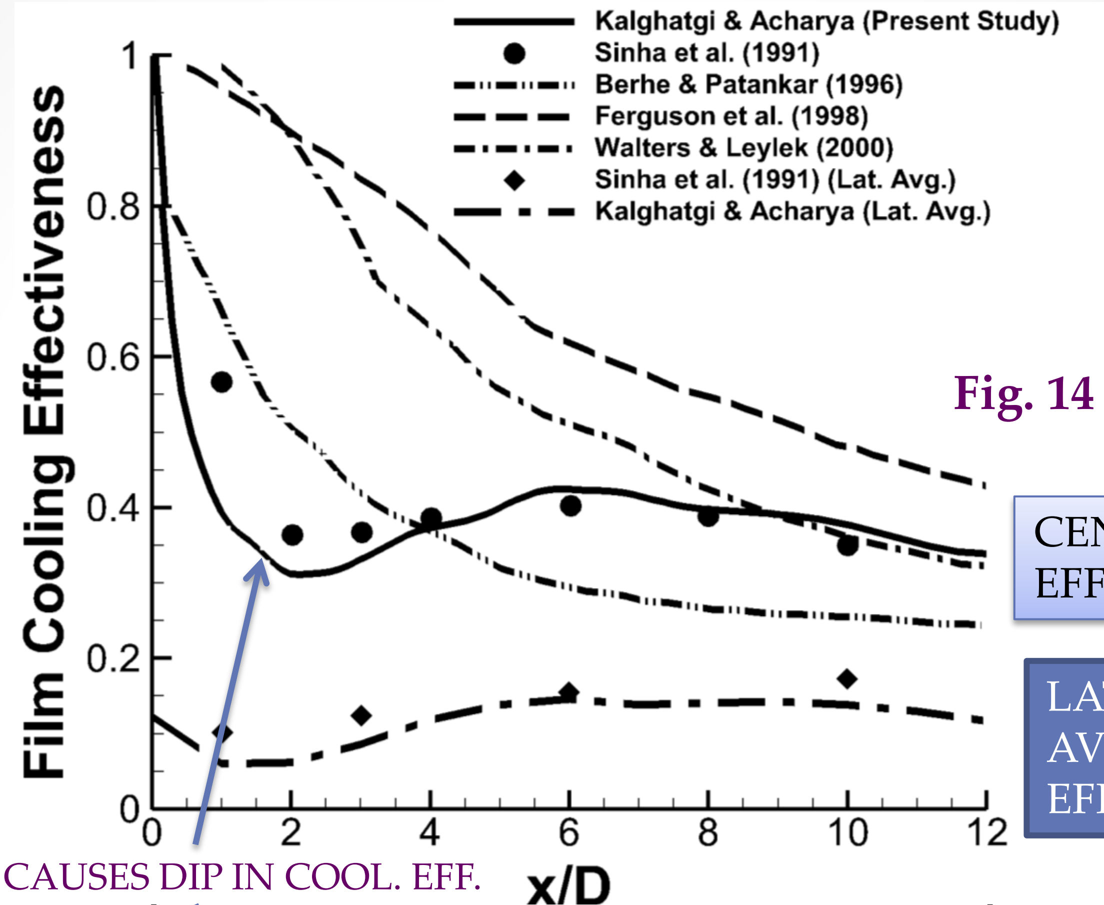

Fig. 14

CENTERLINE EFFECTIVENESS

LATERALLY-AVERAGED EFFECTIVENESS

DETACHED REGION CAUSES DIP IN COOL. EFF.

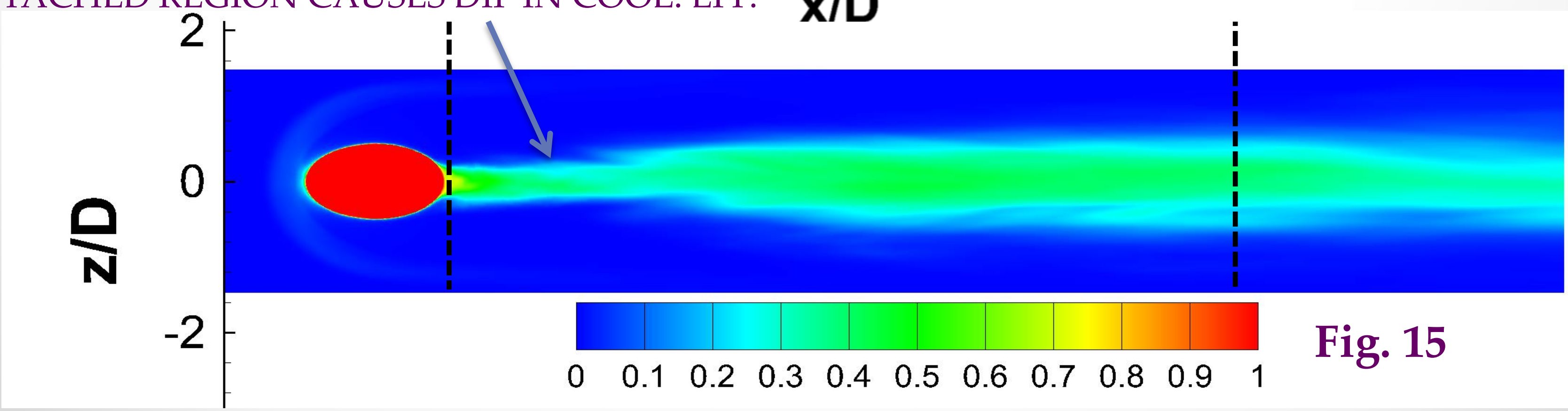

Fig. 15

Outline

- Introduction
- Film Cooling Physics *(Kalghatgi & Acharya (ASME J. Turbomachinery, 2013))*
  - Coherent flow structures
  - Modal analysis
- Film Cooling Geometry
  - *ASME Turbo Expo 2014*
- Blowing Ratio Uncertainty-Quantification
  - *J. Heat Transfer 2013*
- Conclusions

Coherent flow structures in film cooling

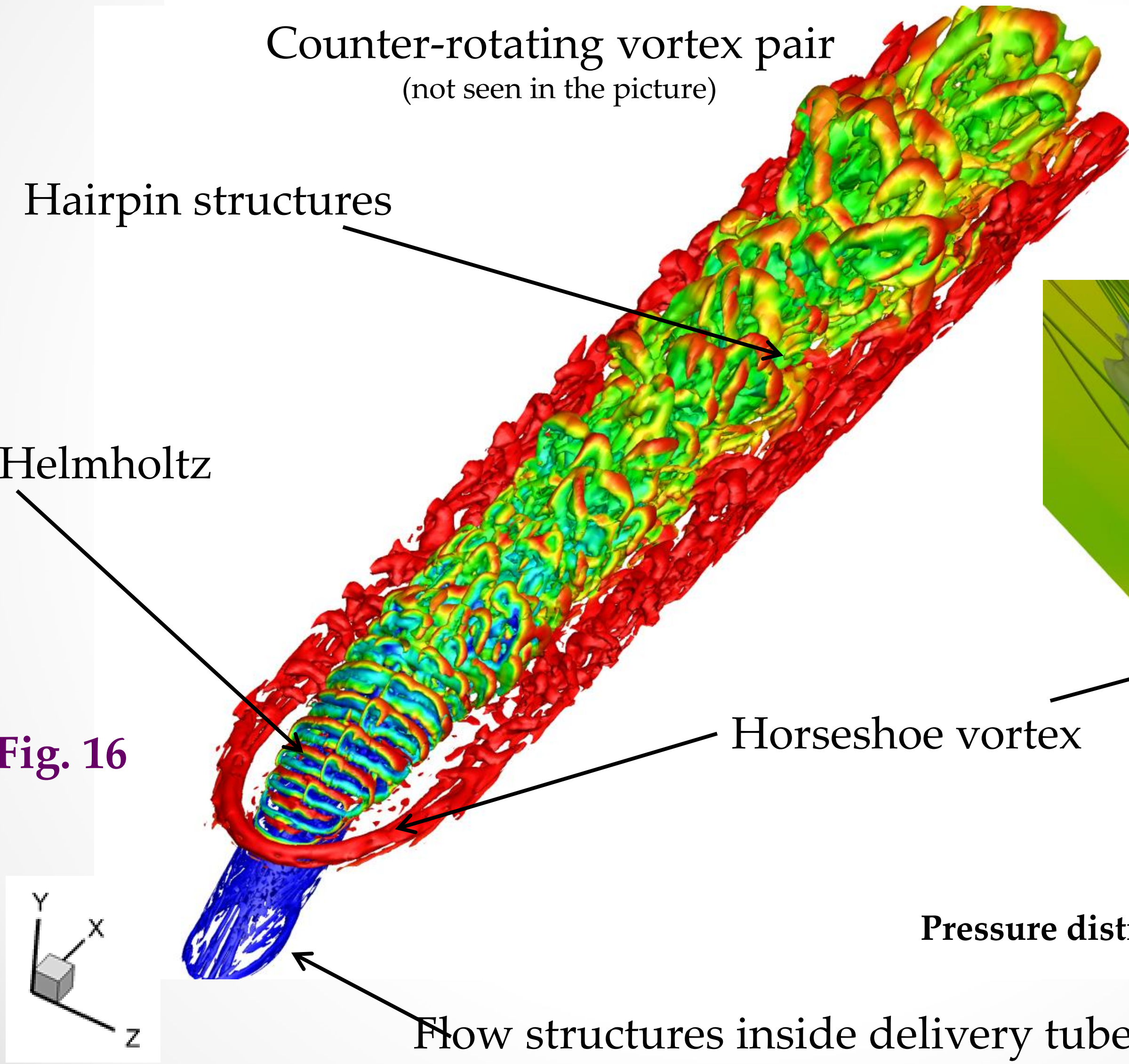

Counter-rotating vortex pair
(not seen in the picture)

Hairpin structures

Kelvin-Helmholtz

Fig. 16

Horseshoe vortex

Flow structures inside delivery tube

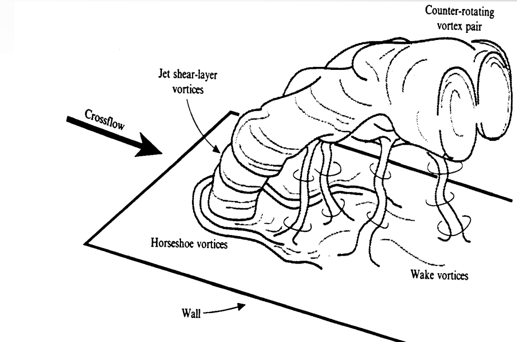

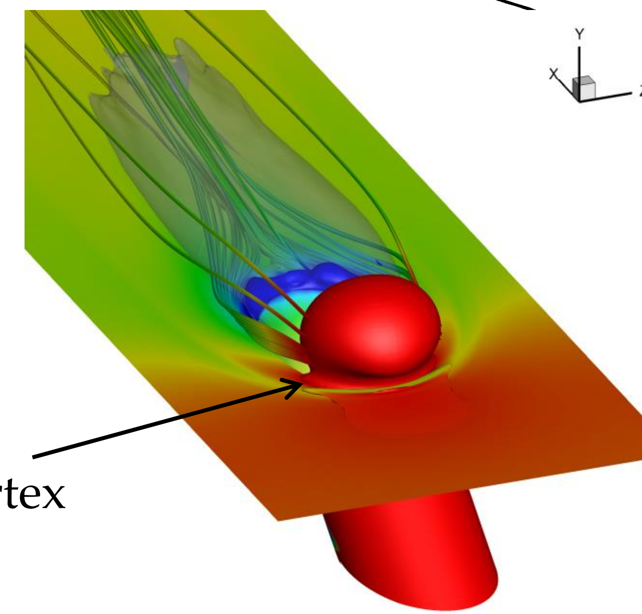

Pressure distribution across the jet and streamlines

Kelvin-Helmholtz mechanism

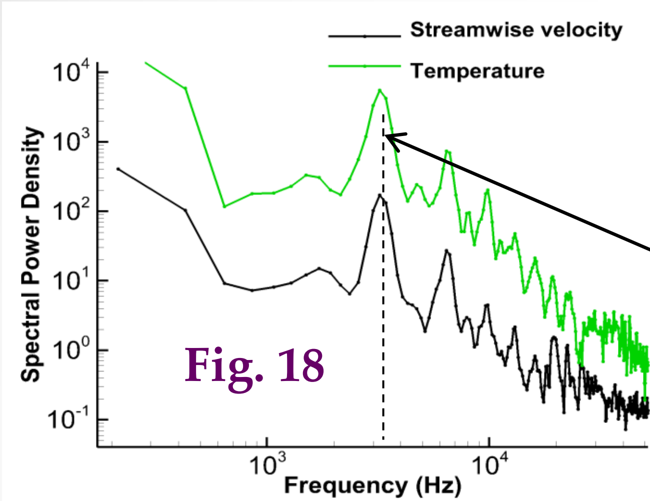

Fig. 18

Peak frequency of K-H mechanism 3180Hz (St_θ=0.125) θ - momentum thickness at x/D = -1

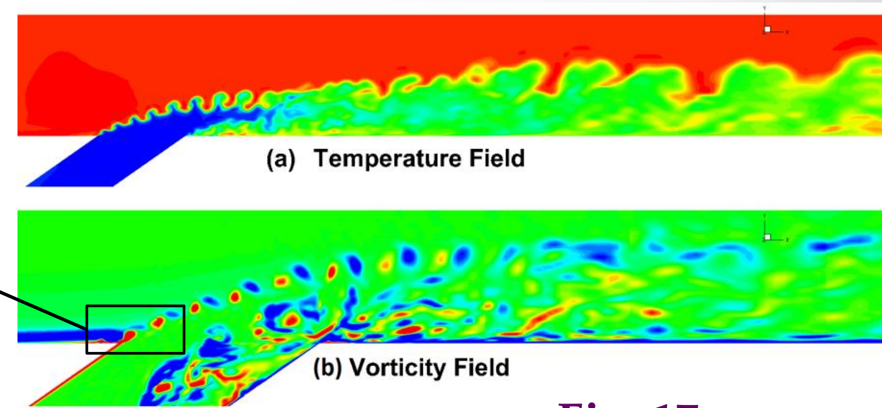

Fig. 17

Instantaneous temperature and vorticity field

(a) (b) Snapshot Δt = 0.8μs (c) (d)

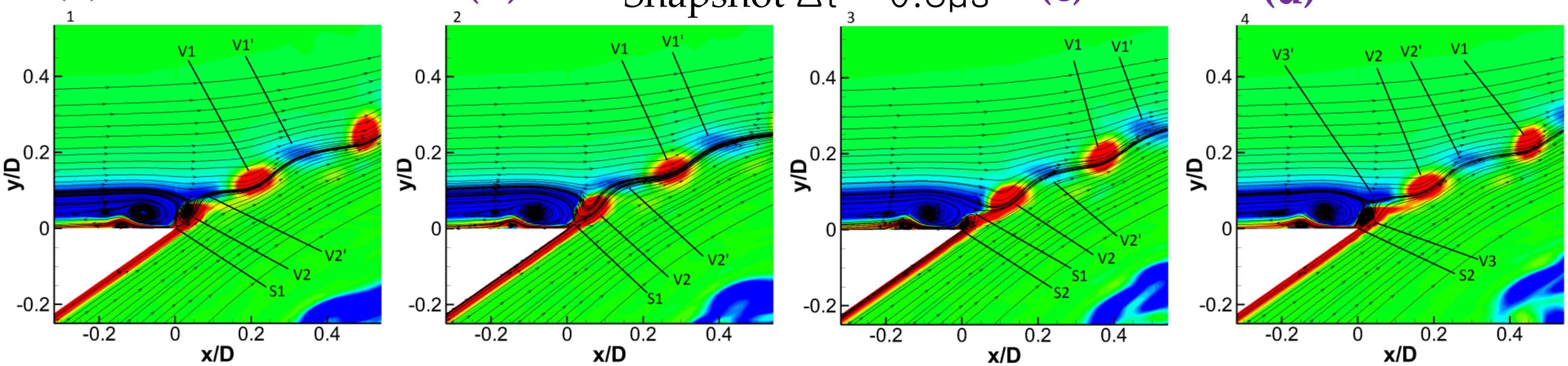

Shedding of K-H vortices over one frequency cycle

Fig. 19

S – Local stagnation point, V – Clockwise (Positive vortex), V' – Counterclockwise vortex

K-H structures and evolution of CVP-I

(a)

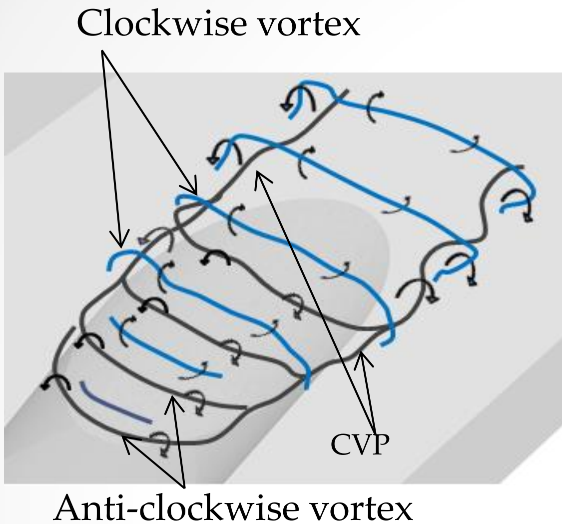

Initial development of CVP: amalgamation of streamwise swept legs of K-H vortices

(b)

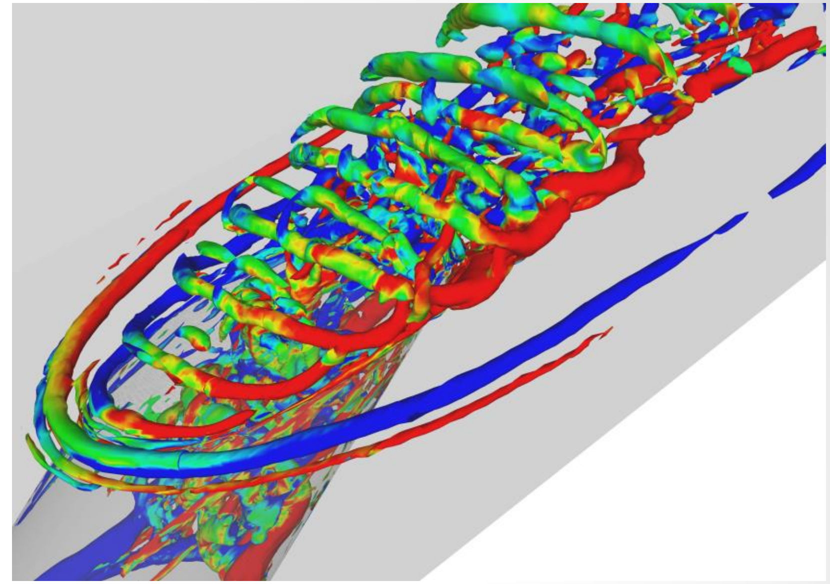

K-H Vortices in 3D (Contours – Streamwise vorticity)

(c)

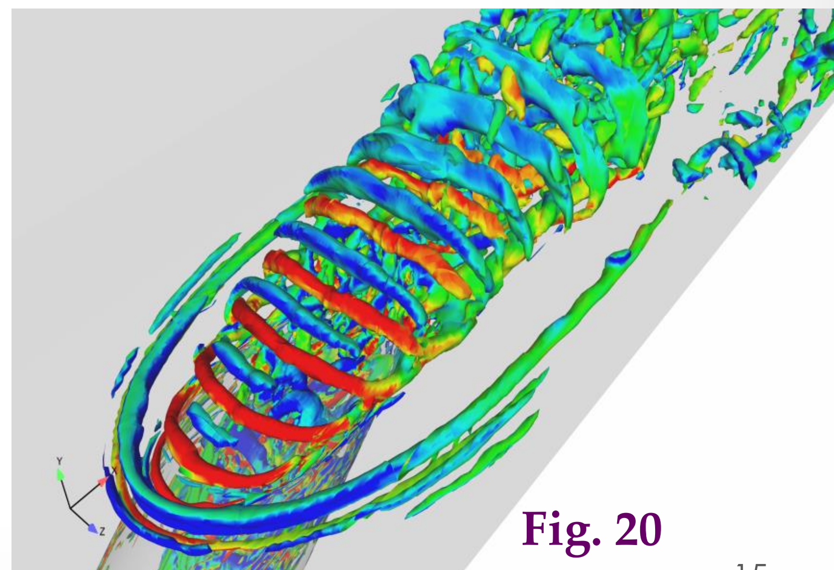

Fig. 20

K-H Vortices in 3D (Contours – Spanwise vorticity)

(d)

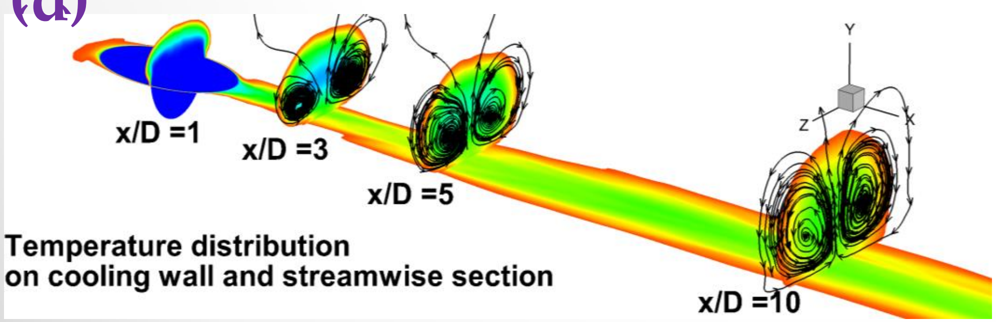

Flow field inside delivery tube & CVP origins-II

- **Spiral structures originates at the lateral ends of delivery tube due to entrance effect**
- **Spiral structures are swept out through exit plane of film cooling hole eventually merging in CVP – short delivery tube effect**
- Hairpin type flow structures superimposed over spiral vortices

(a)

Fig. 22

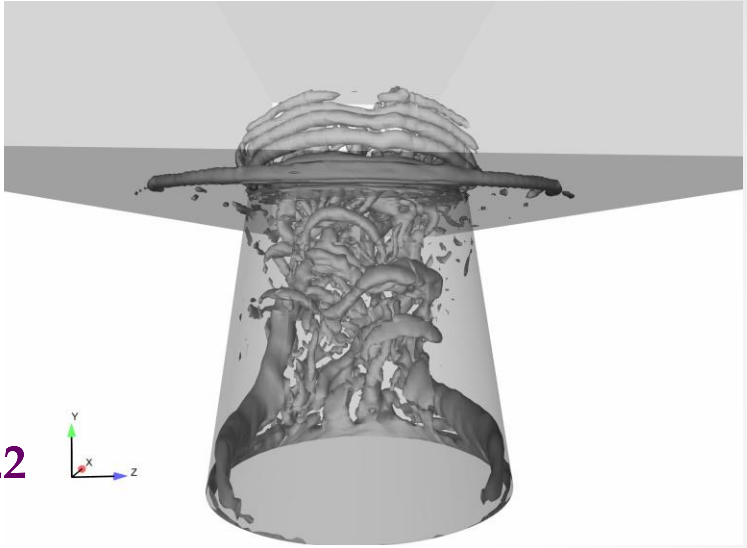

Instantaneous flow structures

(b)

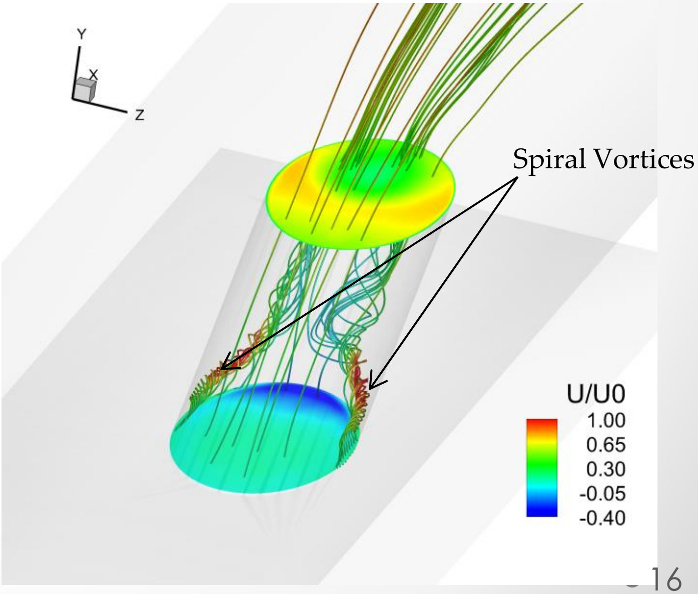

Streamlines in time averaged flow field

CVP Mechanisms- I & II

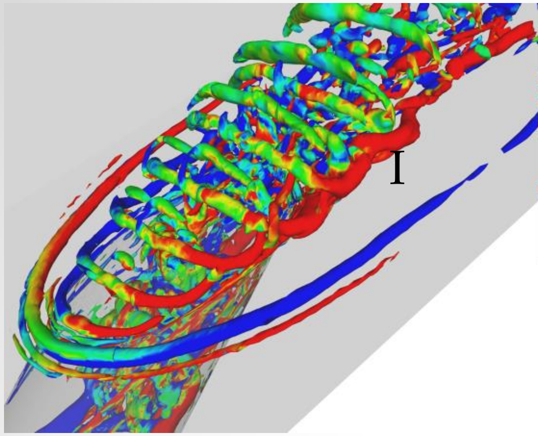

Fig. 23

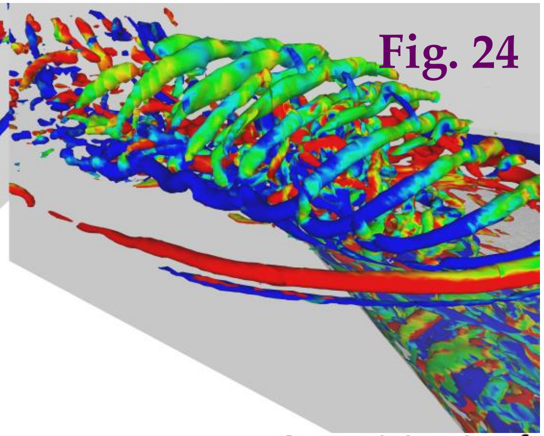

Fig. 24

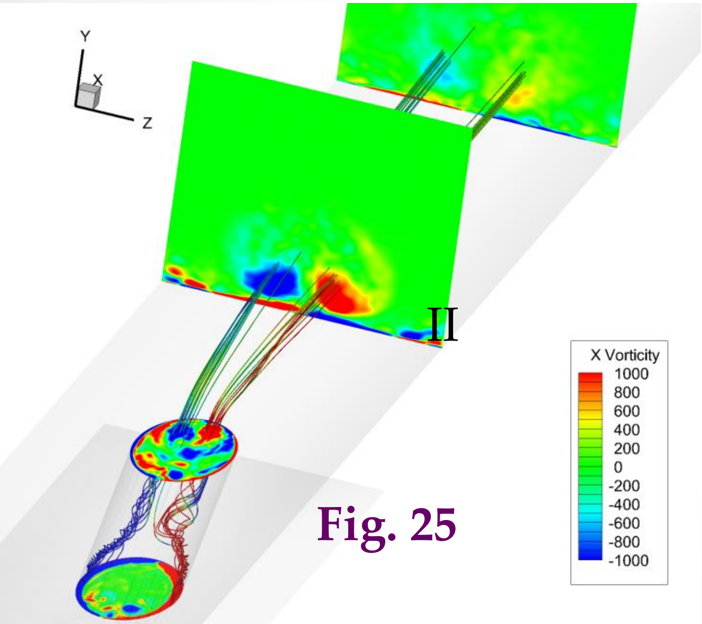

Fig. 25

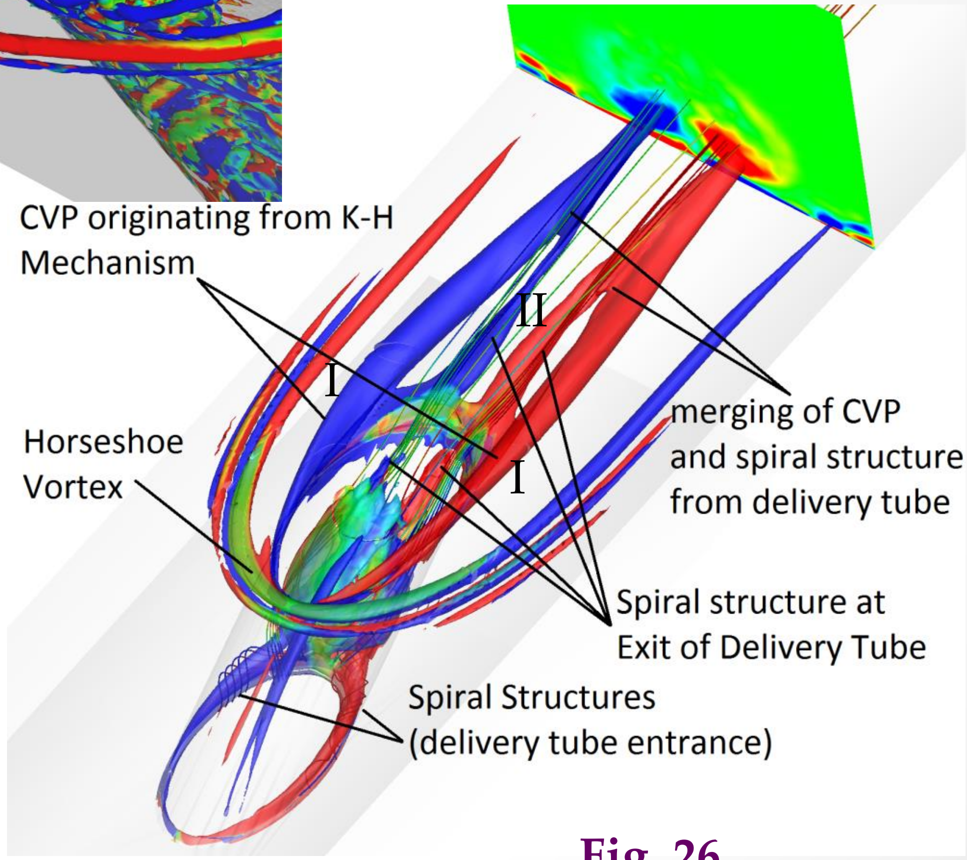

Fig. 26

Modal analysis

Eigen value of S

$\lambda_i = \log(\sigma_i)/\Delta t$

Growth rate = $\mathrm{Re}(\lambda_i)$

Frequency = $\mathrm{Im}(\lambda_i)$

DMD Parameters

Sampling frequency = 25 kHz

Number of snapshots N = 100

Grid points / snapshot ~ 6M

Mode tag	Frequency (Hz)
→ (B)	258
→ (G)	465
O (1-3)	750 - 1208
O (1-6)	1474 - 2762
→ (R)	3180

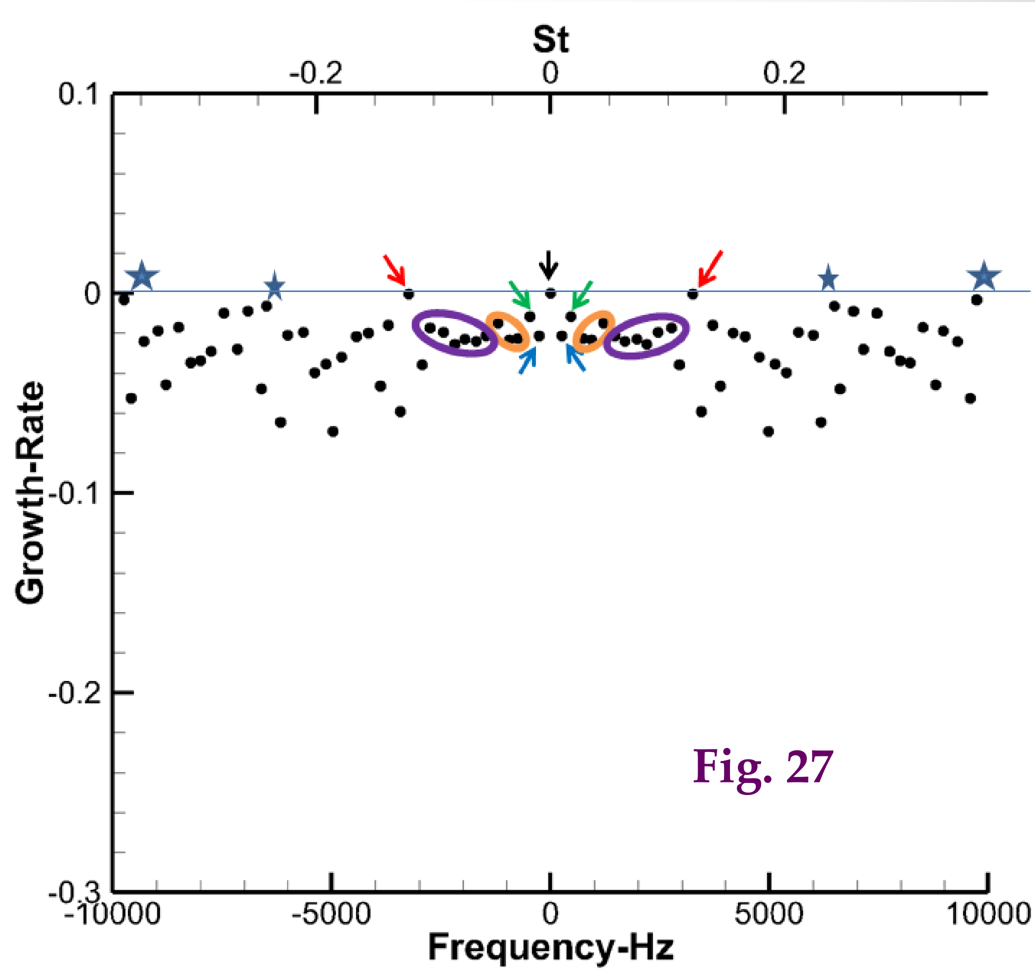

DMD Growth Spectra

Modal energy spectrum

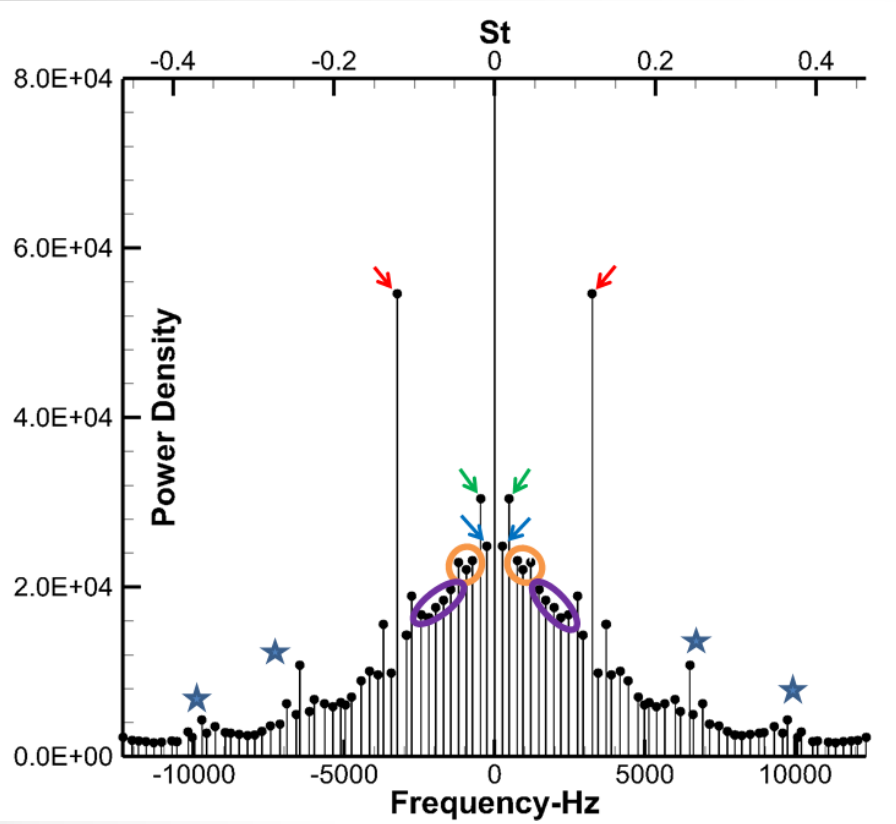

DMD Global Energy spectrum

Fig. 28

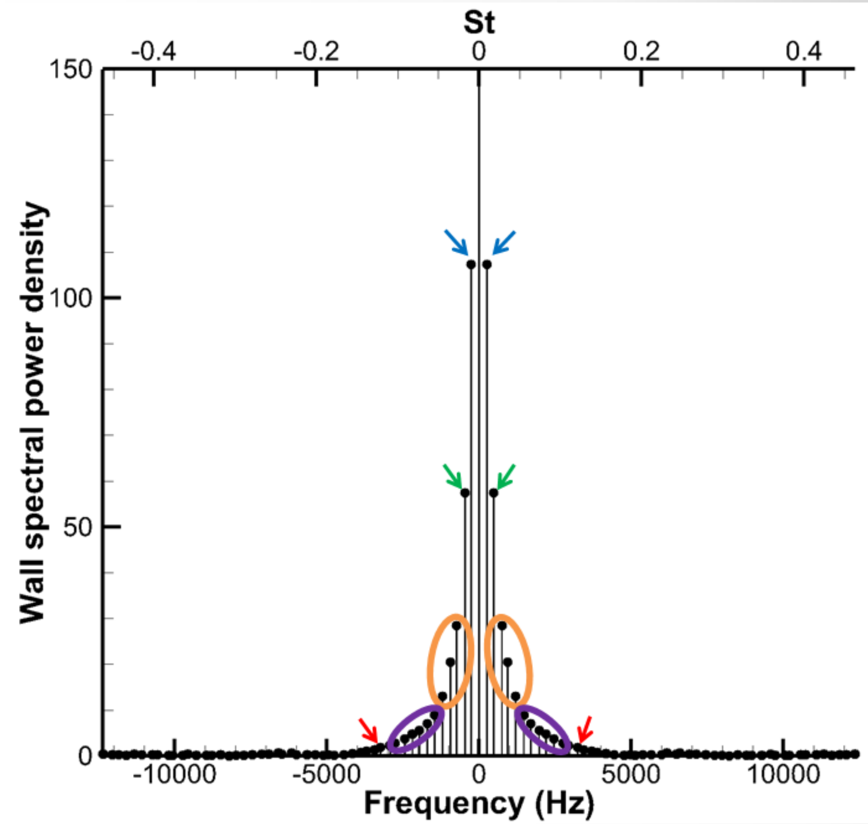

DMD Energy spectrum near the wall

Fig. 29

Mode tag	Frequency (Hz)
→ (B)	258
→ (G)	465
O (1-3)	750 - 1208
O (1-6)	1474 - 2762
→ (R)	3180

Modal contribution to film cooling effectiveness

Mode tag	Frequency (Hz)
→ (B)	258
→ (G)	465
O-1	750
O-2	942
O-3	1208
P-1	1474

Max. RMS

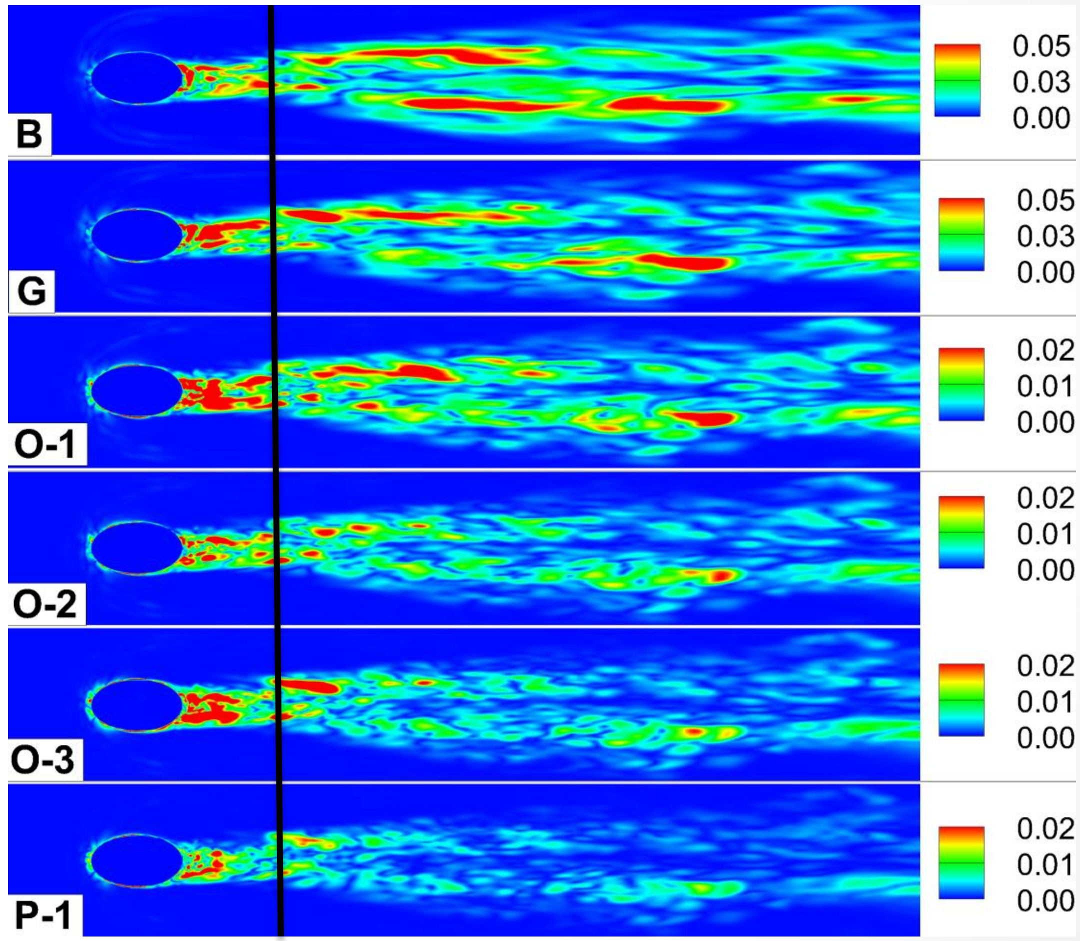

16-18%

5-8%

Fig. 31

Hydrodynamic flow structures

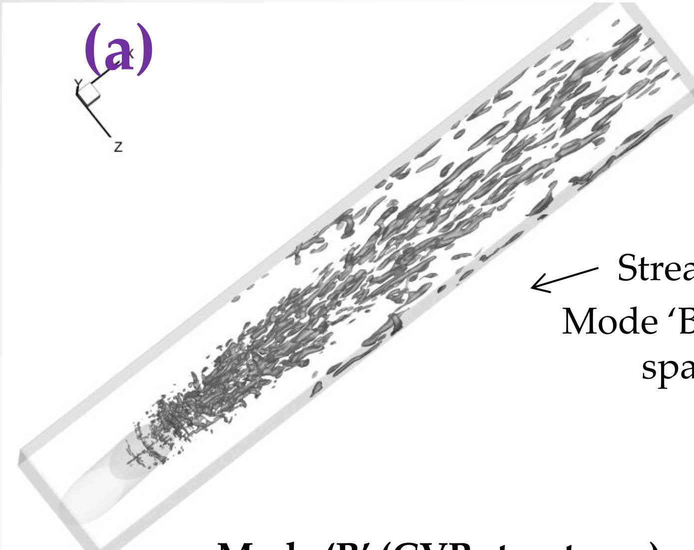

Mode 'B' (CVP structures)

Streamwise flow structures

Mode 'B' and 'G' are similar – spanwise structures

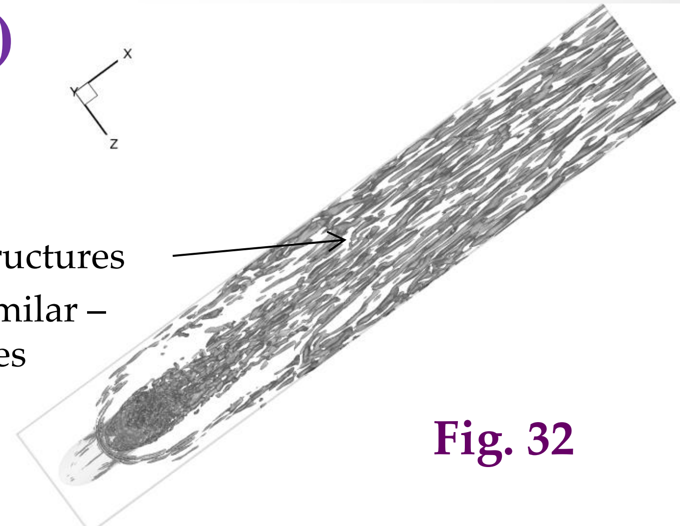

Mode 'B' (wall structures)

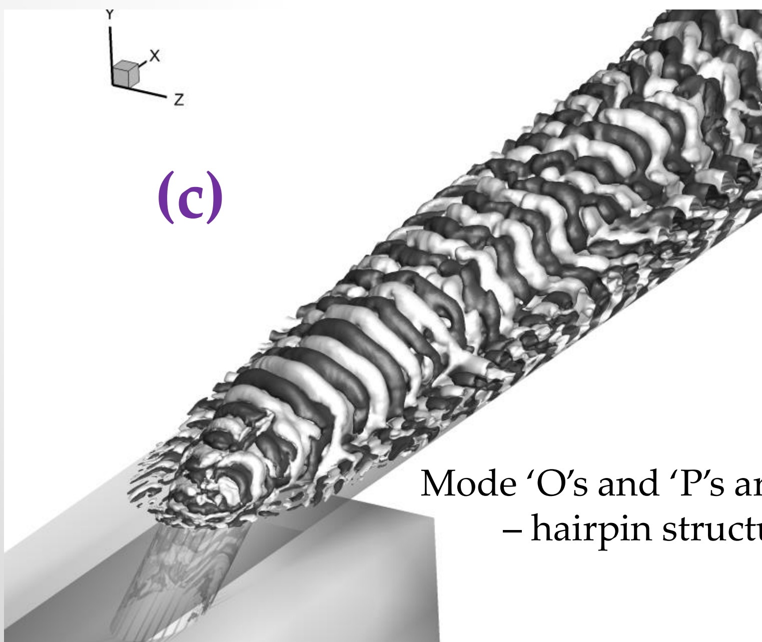

Mode 'O's and 'P's are similar – hairpin structures

Mode 'O-1' – hairpin structures

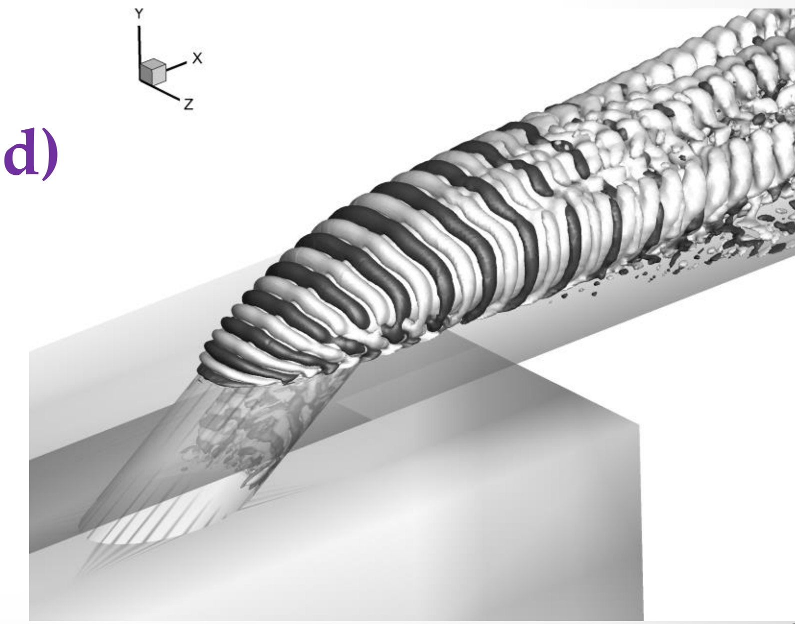

Mode 'R' – Kelvin Helmholtz

Outline

- Introduction
- **Film Cooling Physics**
  - **Coherent flow structures**—Identified key mechanisms for CVP formation and the important role of in-hole structures (not known before)
  - **Modal analysis**– identified the various modes that contribute to the film cooling distributions, and the discovery that the low frequency streamwise-oriented structures near the wall have the strongest effect on film cooling. This understanding was completely missing from the literature.
  - Q- Since specific coherent modes and their energy control the near-surface mixing and heat transfer, can geometry modifications be used to beneficially alter these modes?
- **Film Cooling Geometry**
  - ***ASME Turbo Expo 2014 (Kalghatgi & Acharya, 2014)***
- Blowing Ratio Uncertainty-Quantification
  - *J. Heat Transfer 2013*
- Conclusions

Background: Shape modification for enhanced performance

Film cooling with shaped holes

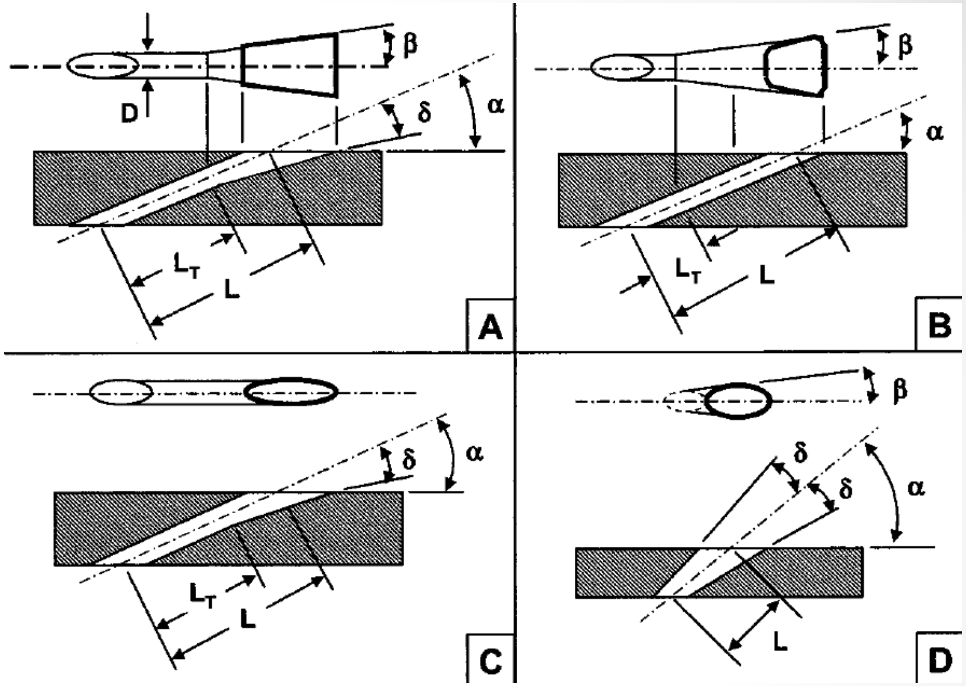

Bunker et. al. 2002

Film cooling holes embedded in craters and trenches
– designs show best performing configurations at 0.75D depth

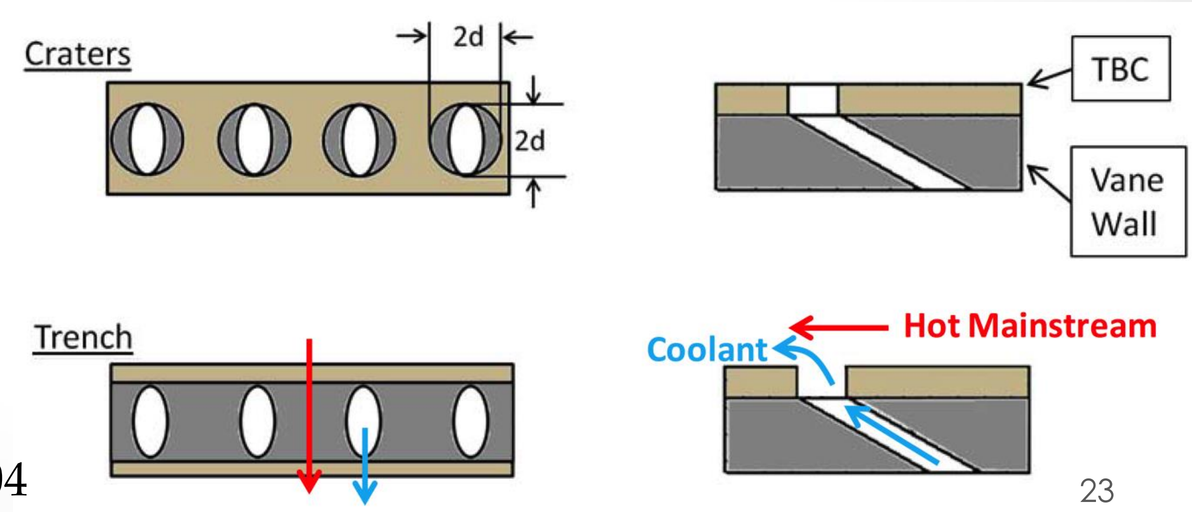

Bogard et. al. 2004

Shaped Holes are Today's Technology

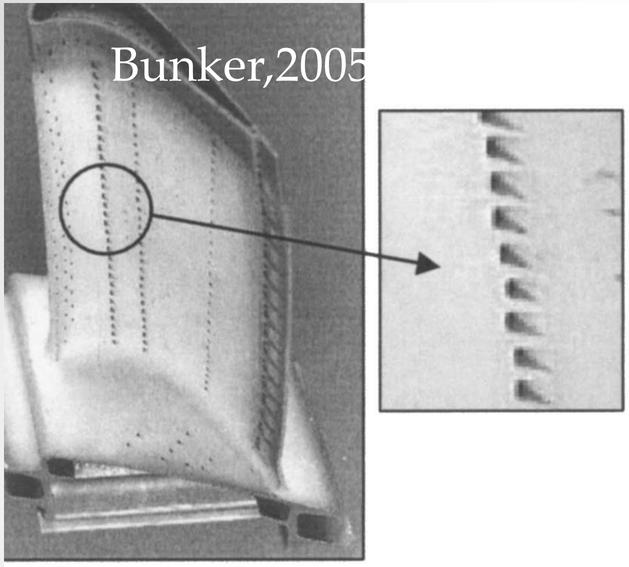

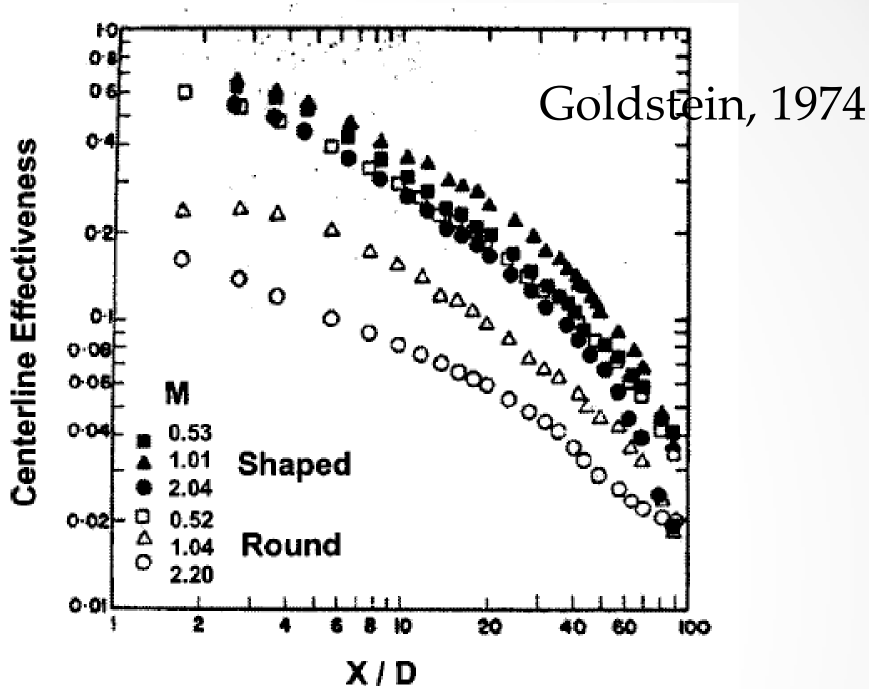

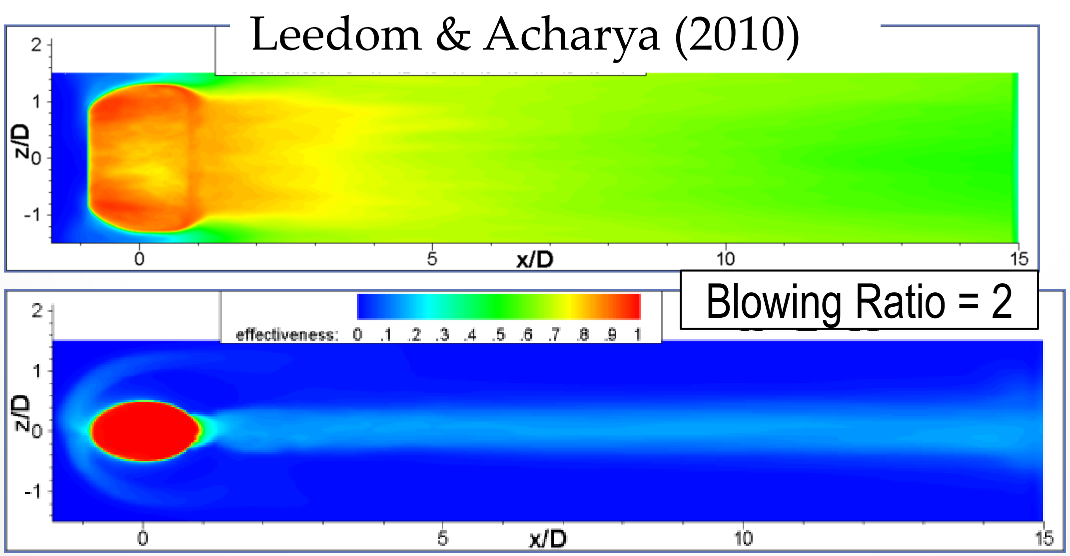

Trenched holes and Cratered holes

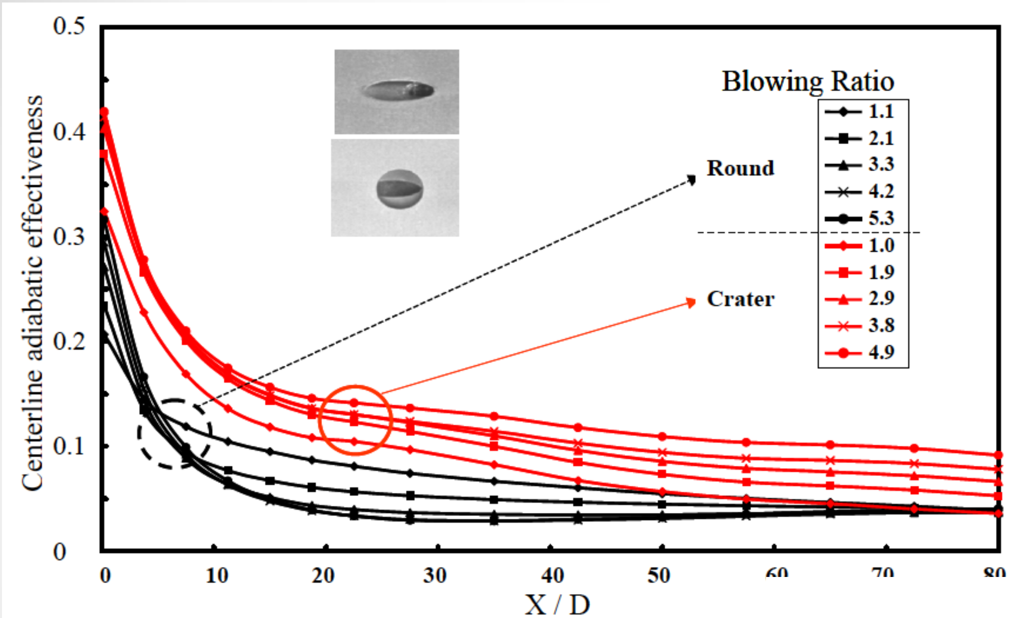

From Bunker, 2009

-Both trenched holes and cratered holes show promise in increasing cooling effectiveness

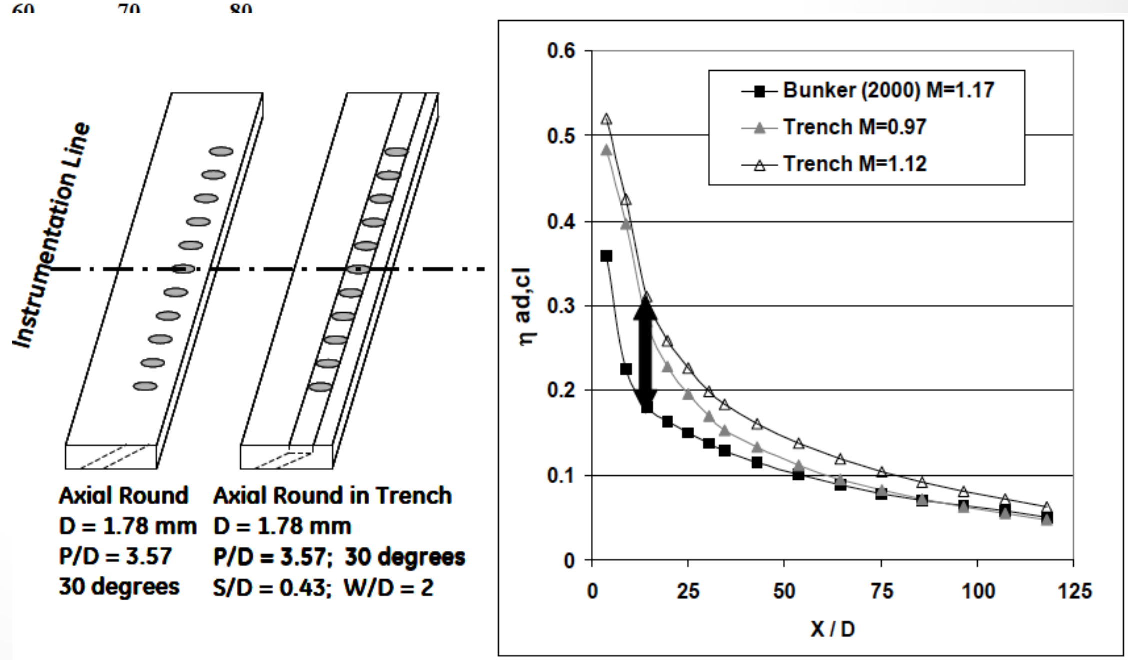

Novel shaped crater design and flow conditions

- The basic idea of a crater is to spread out the coolant film and increase lateral coverage
- The crater is usually created in the TBC on the airfoil
- **The novel design attempts to modify the flow structures by introducing an anti-CRVP**
- Crater depth is a key parameter

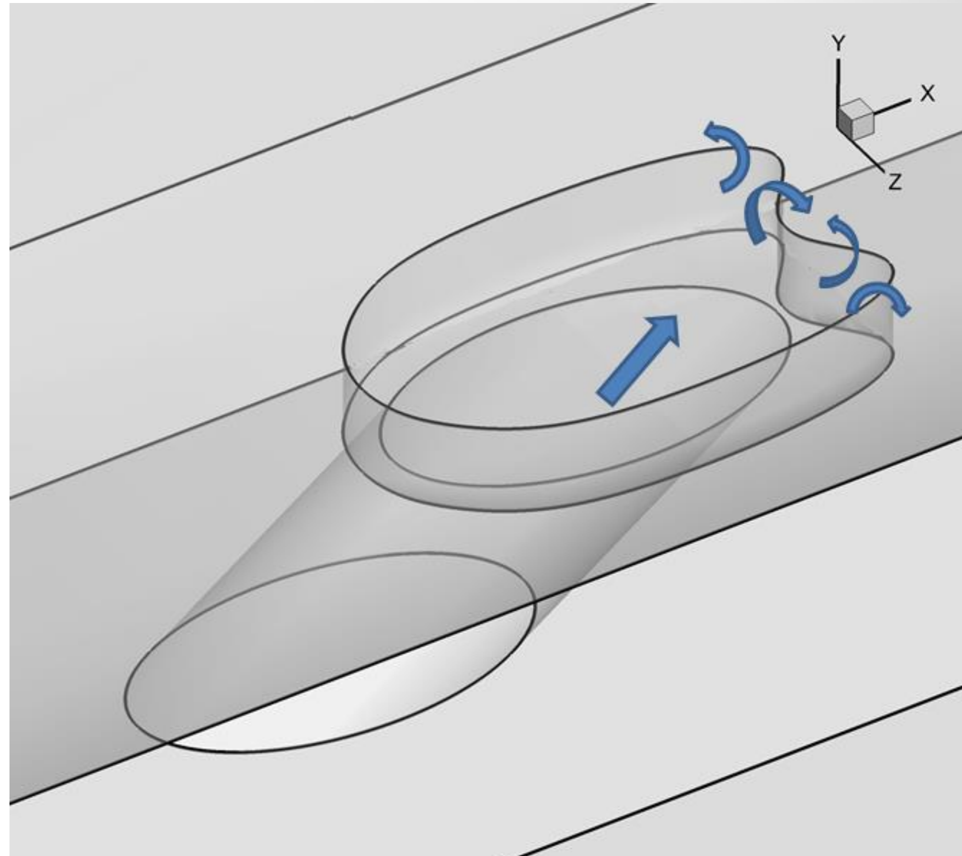

Cases	Depth
Baseline case	0.0D
Case-1	0.2D
Case-2	0.4D
Case-3	0.75D

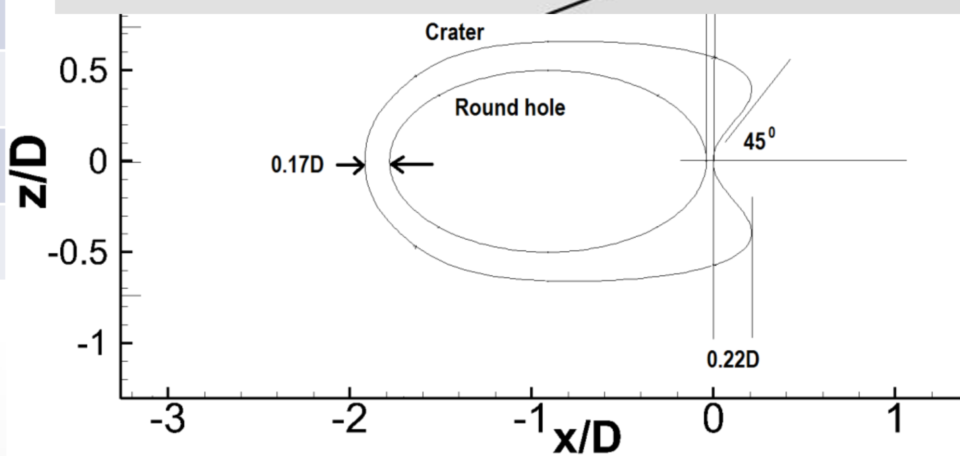

Schematic of flow structures in round film cooling hole and shaped crater: The role of anti—CRVP and Tornado-like Structures

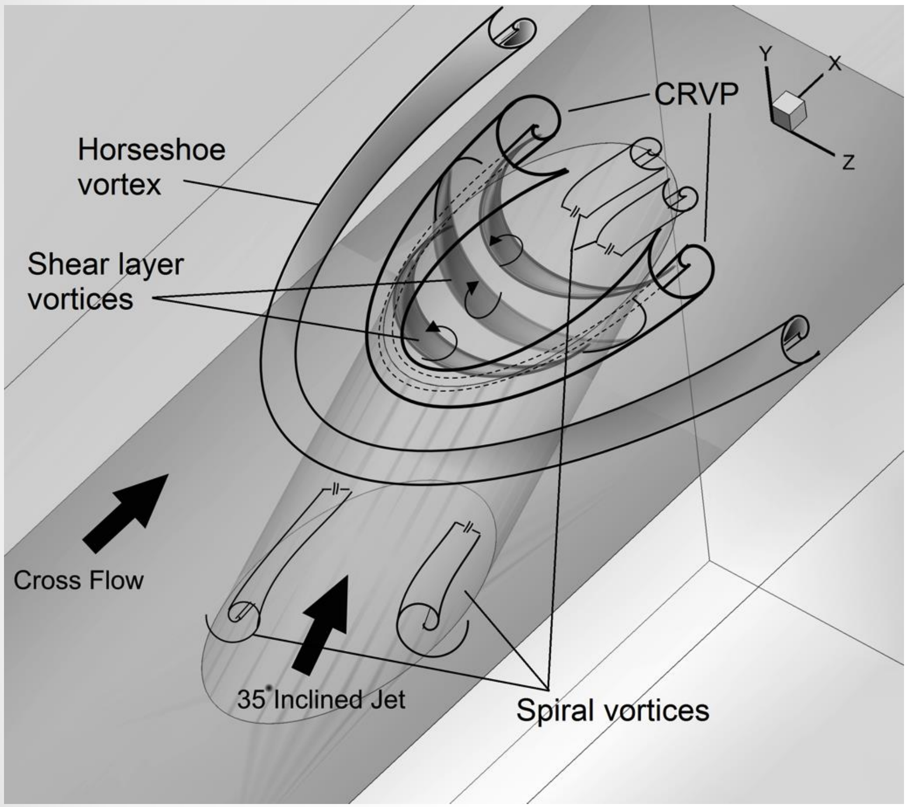

Baseline round hole

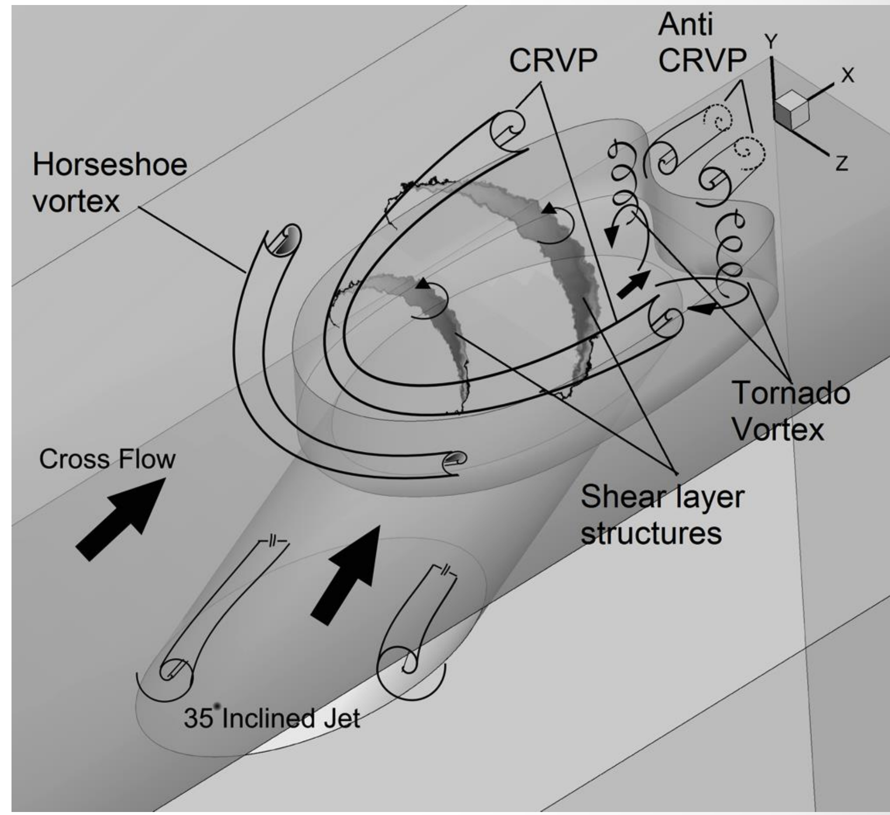

Shaped crater

Instantaneous flow field-X vorticity: Origins of the CRVP

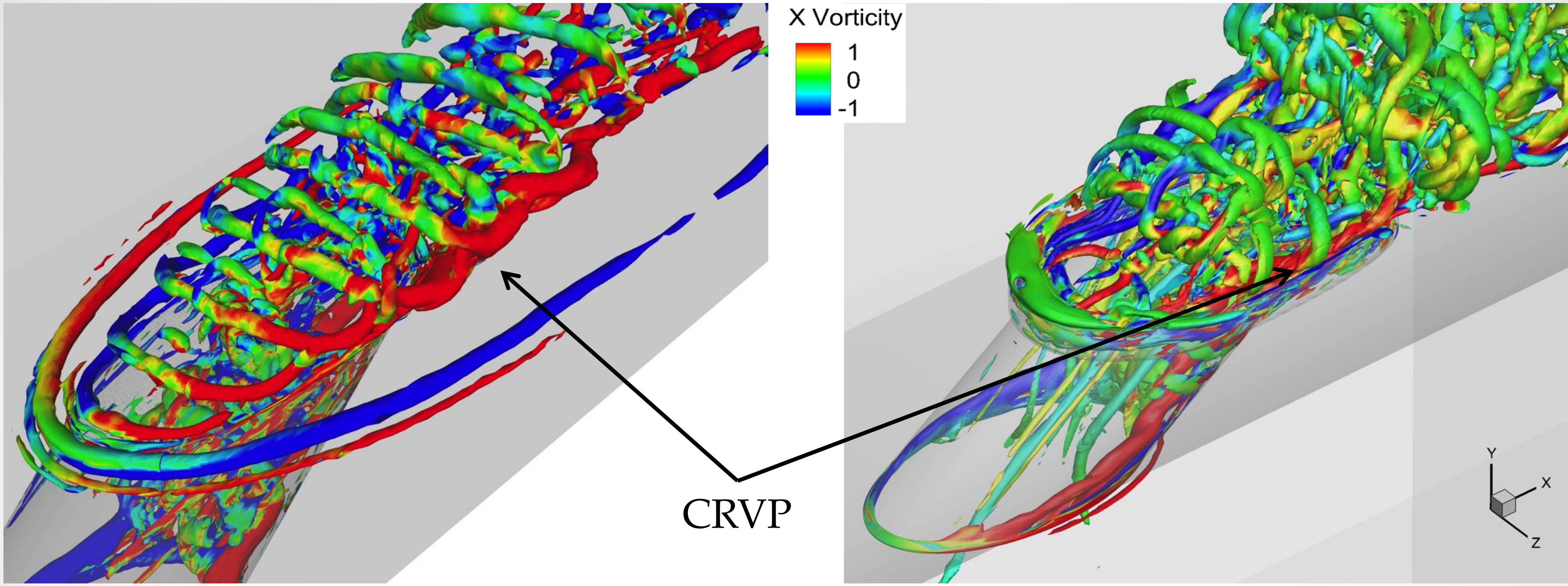

Instantaneous structures in round hole film cooling

Instantaneous structures in round hole embedded in craters

(c)

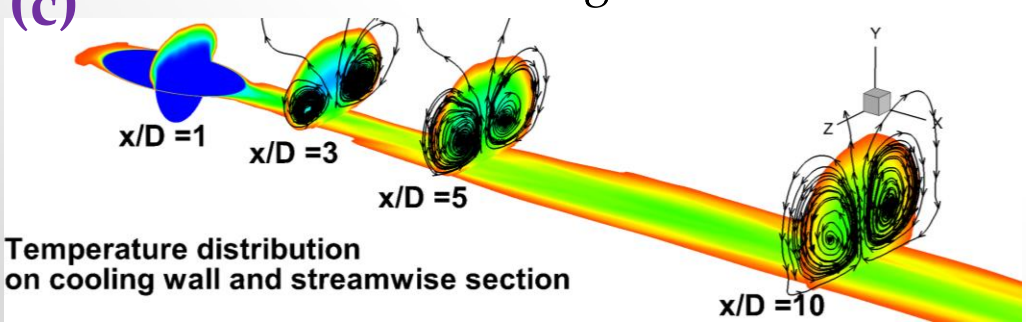

Flow structures for baseline round hole and shaped crater hole

Counter rotating vortex pair

Baseine round hole

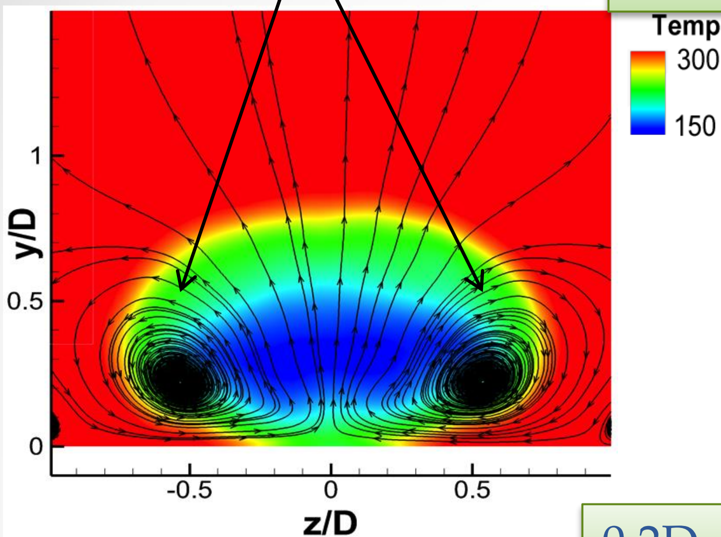

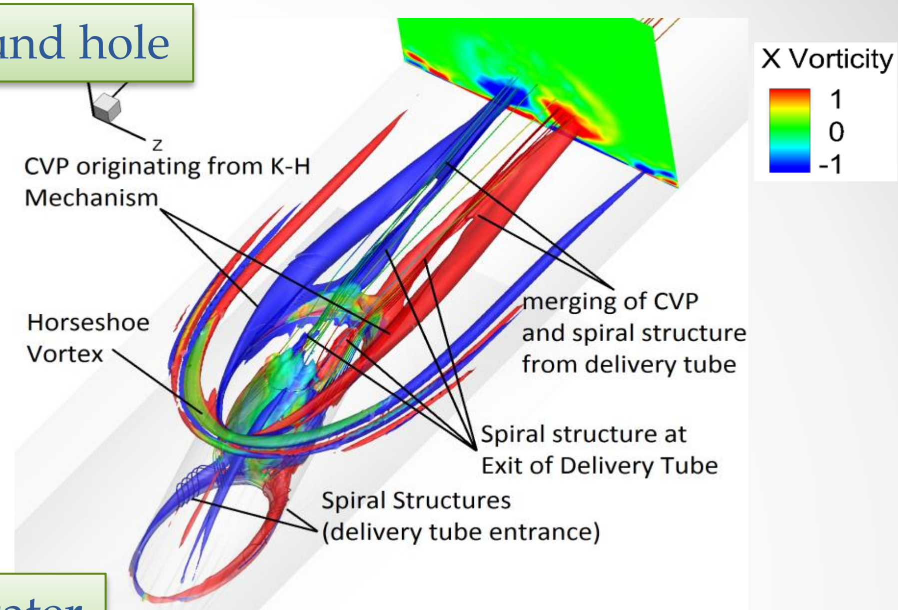

CVP Structure

0.2D deep crater

Counter rotating vortex pair

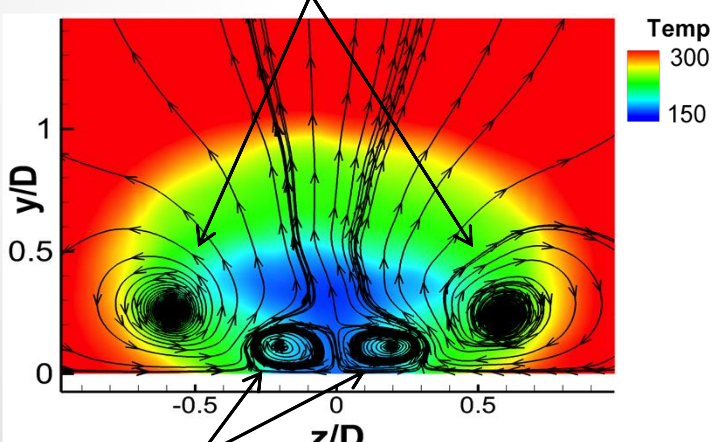

Anti-Counter rotating vortex pair

Counter rotating vortex pair

Anti-Counter rotating vortex pair

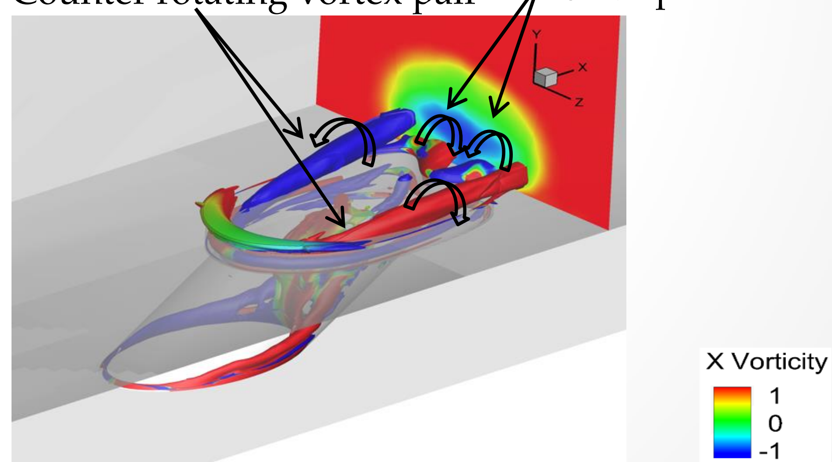

Spiral vortices

Spiral structures are completely neutralized by anti-CVP structures

CVP and anti-CVP for 0.4D deep crater

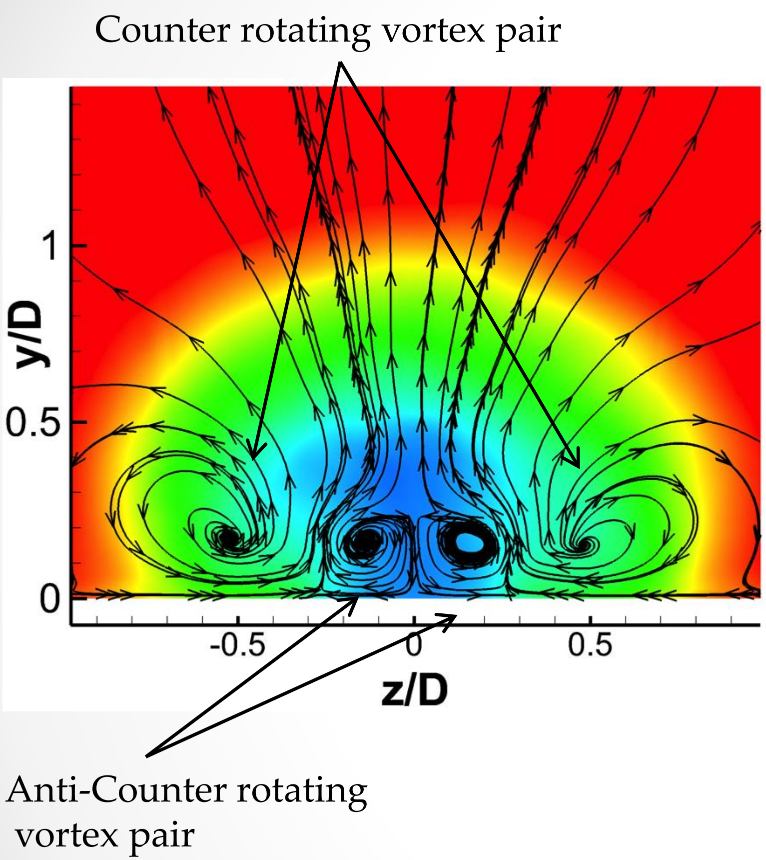

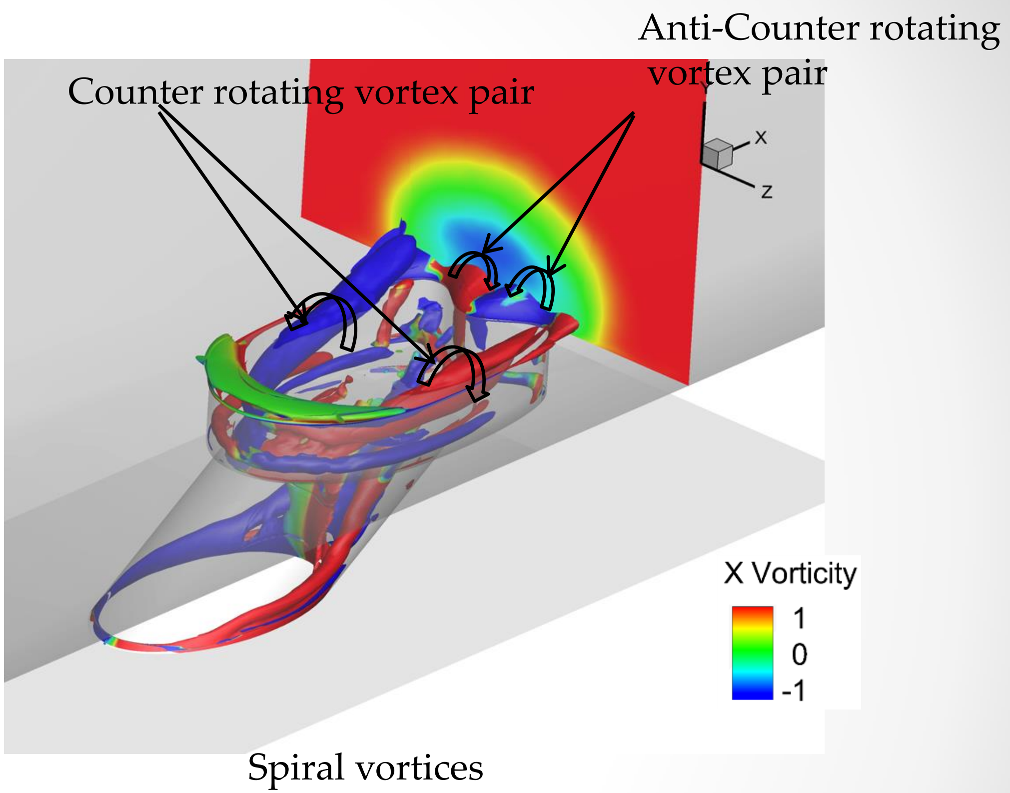

Deep craters attenuates CVP structures

CRVP and anti-CRVP for 0.75D deep crater: The effect of V-protrusion and crater depth

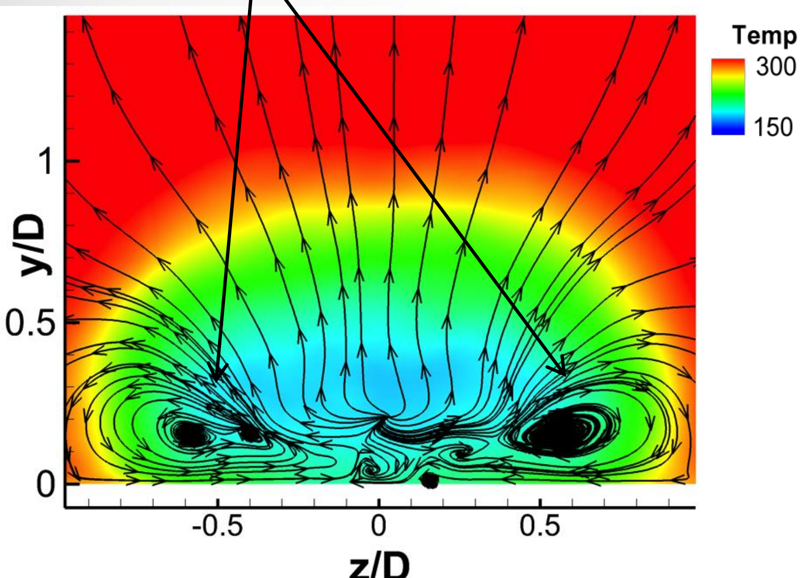

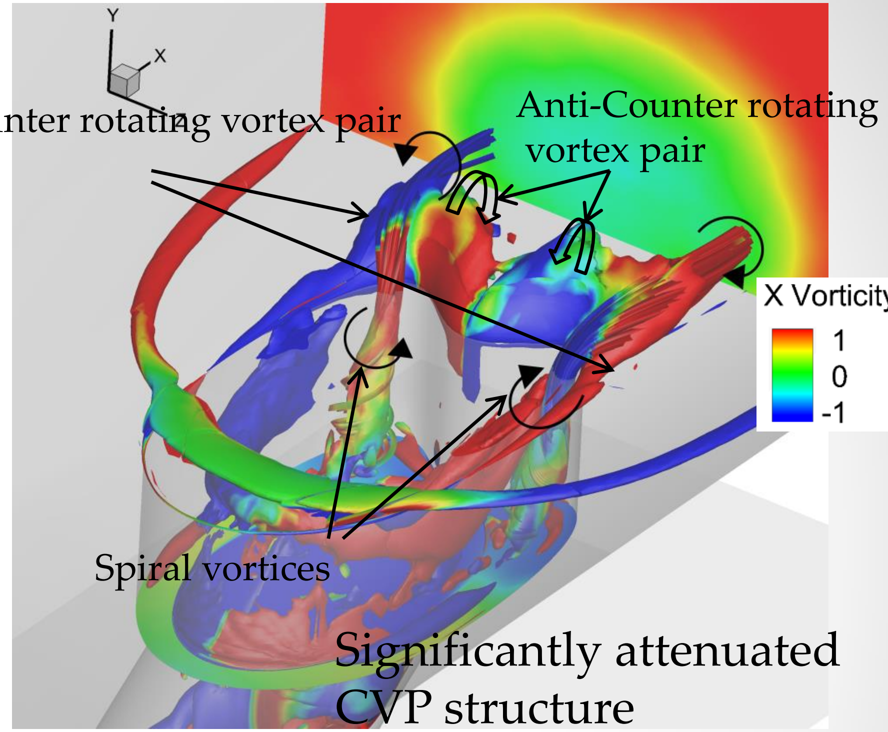

Streamlines & x-vorticity CRVP structures

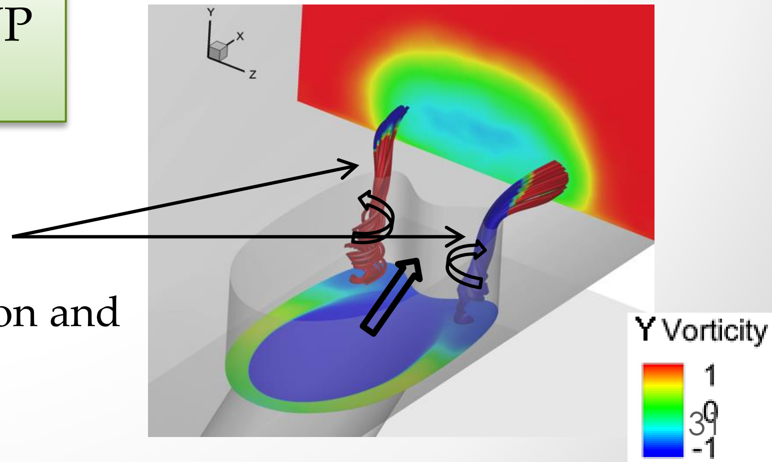

Effect of v-protrusion and crater depth

Spectral Behavior

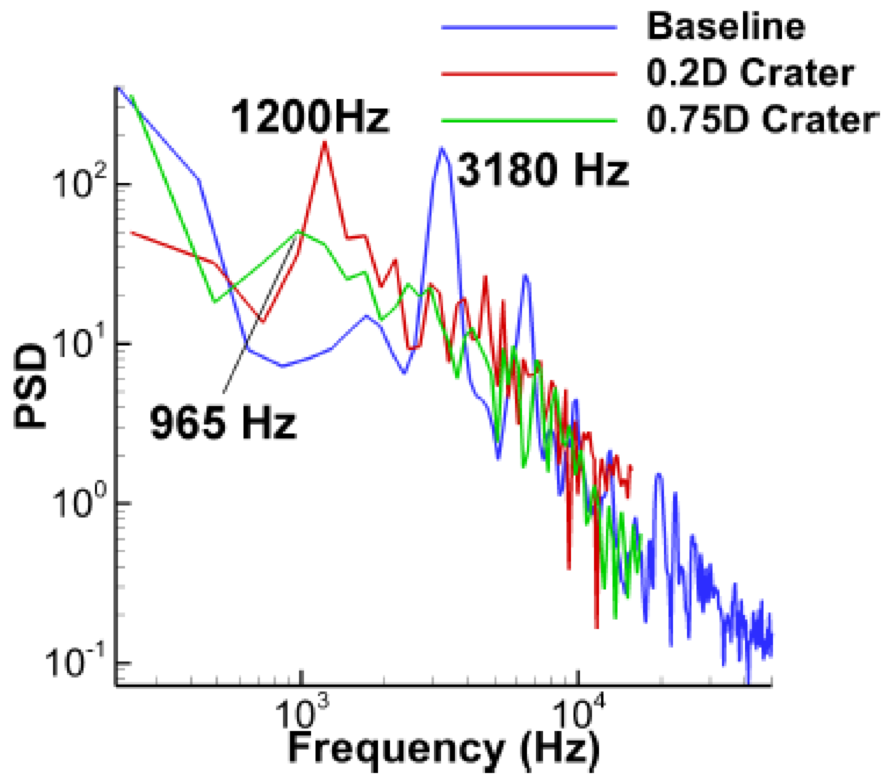

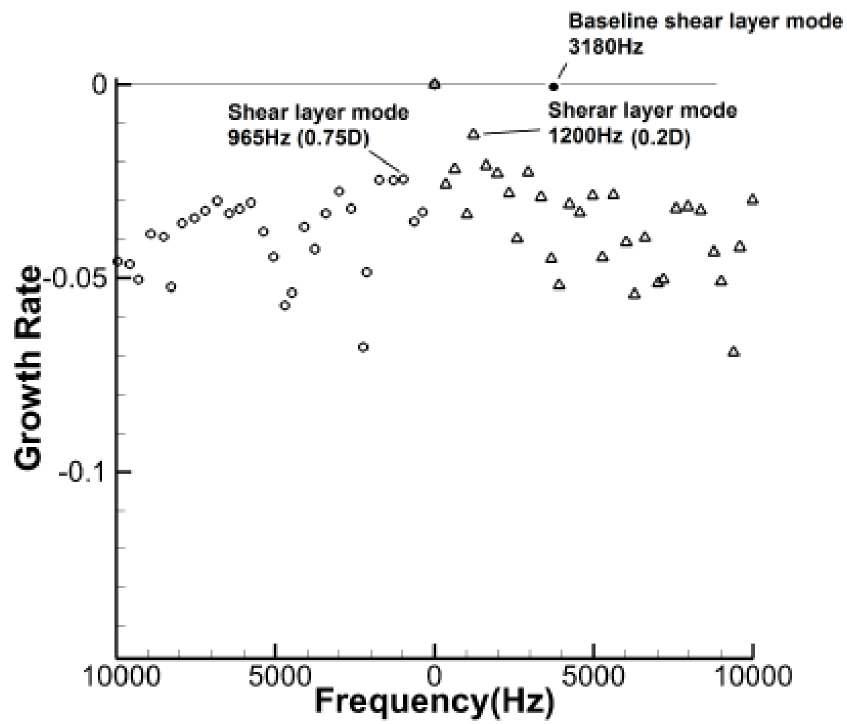

- Baseline case shows strong spectral peaks and harmonics. Significant growth/amplitude at the dominant frequencies
- 0.75D crater case exhibits spectral broadening, absence of dominant peaks and lower growth rates

Modal energy spectrum

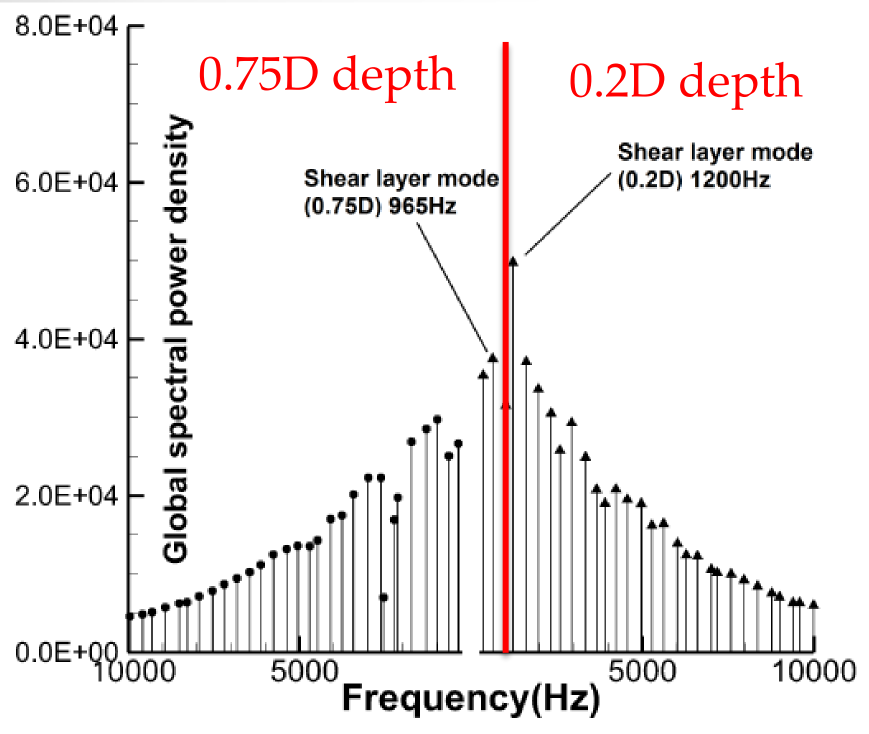

DMD Global Energy spectrum

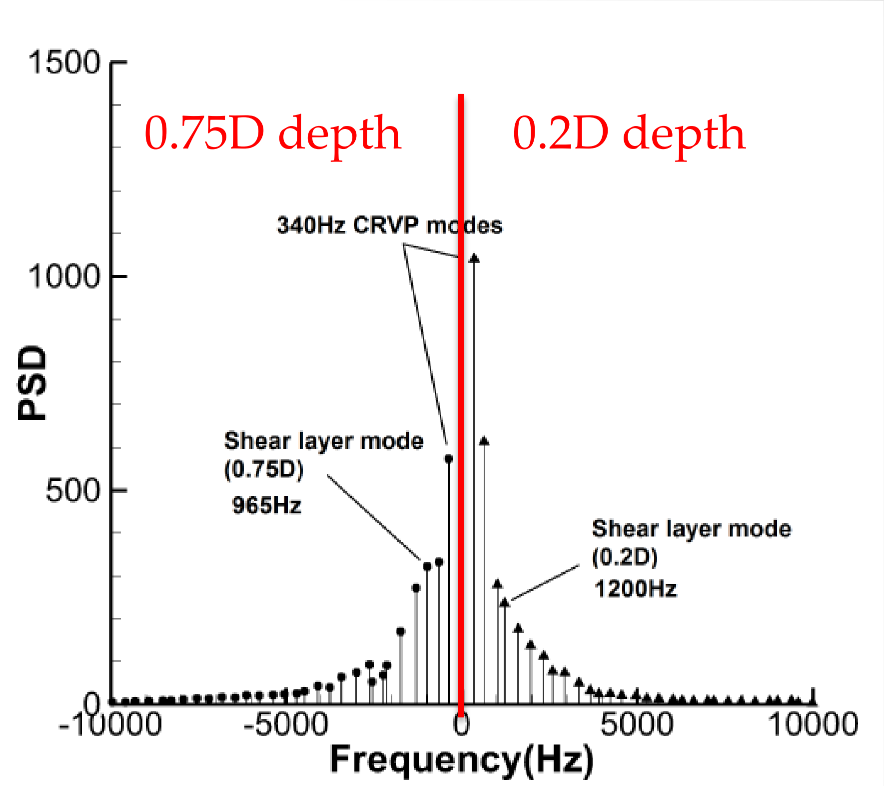

DMD Energy spectrum near the wall

- Global energy spectrum of the cratered holes show lower frequency and less energetic modes relative to the baseline case
- Near-Wall dominant modes are at the lower frequency of 340 HZ

Film cooling effectiveness

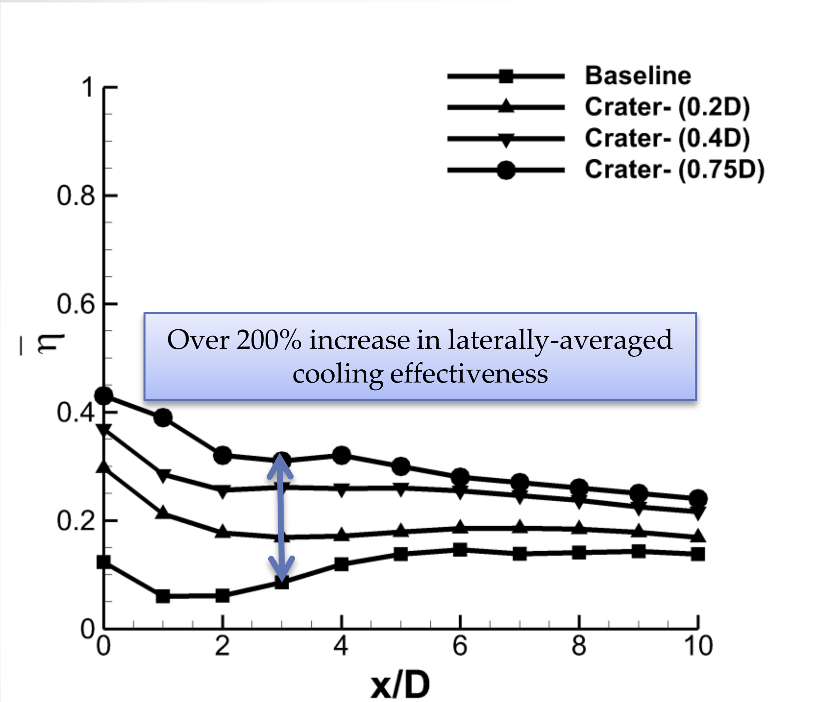

Laterally averaged film cooling effectiveness

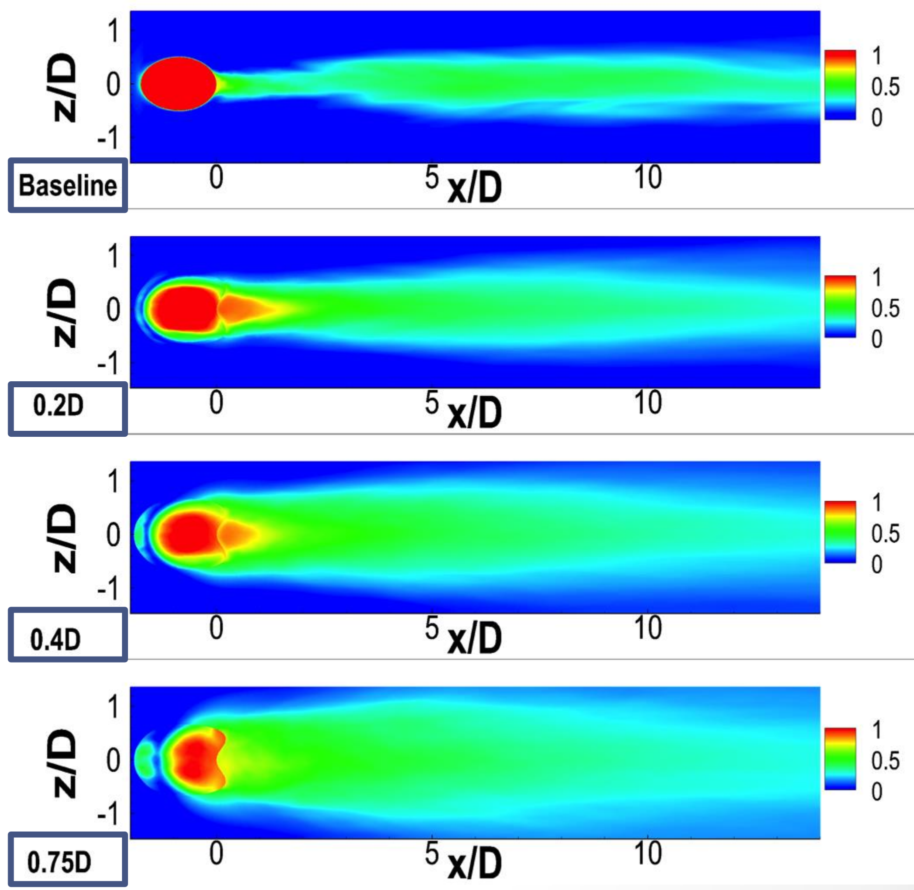

Heat transfer coefficient

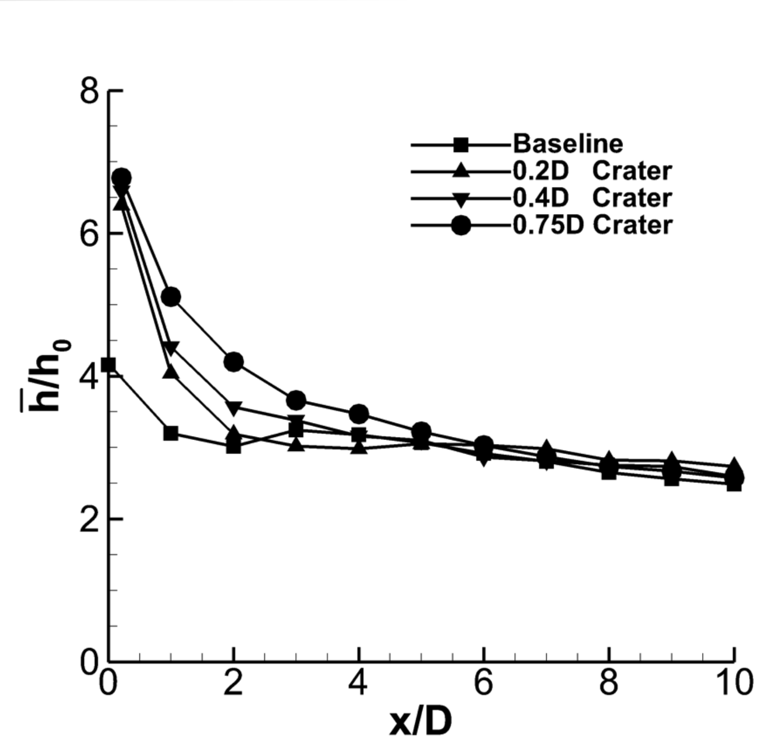

Laterally averaged heat transfer coefficient

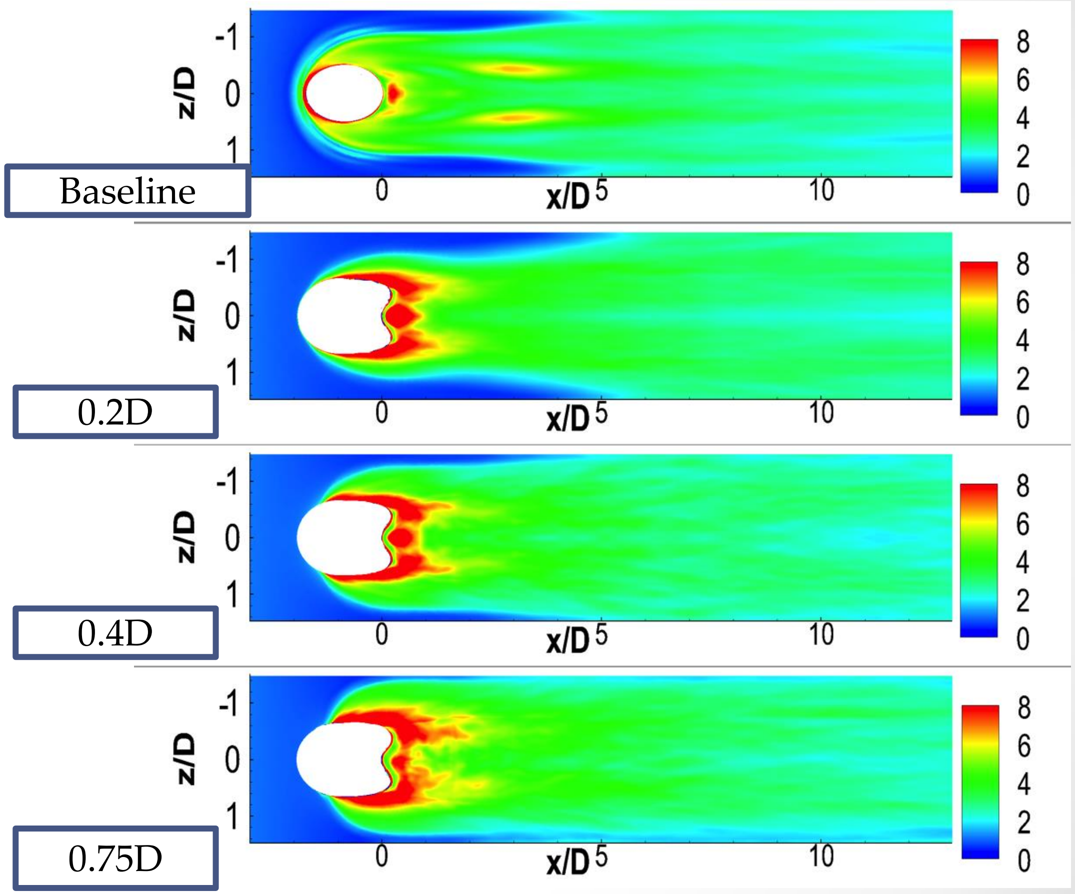

Comparison with conventional designs

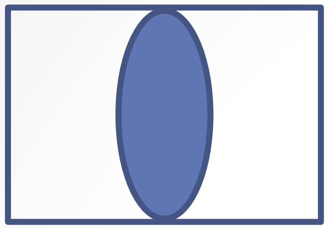

Trench

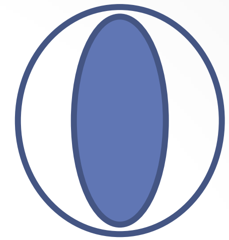

Crater

Best performing conventional designs

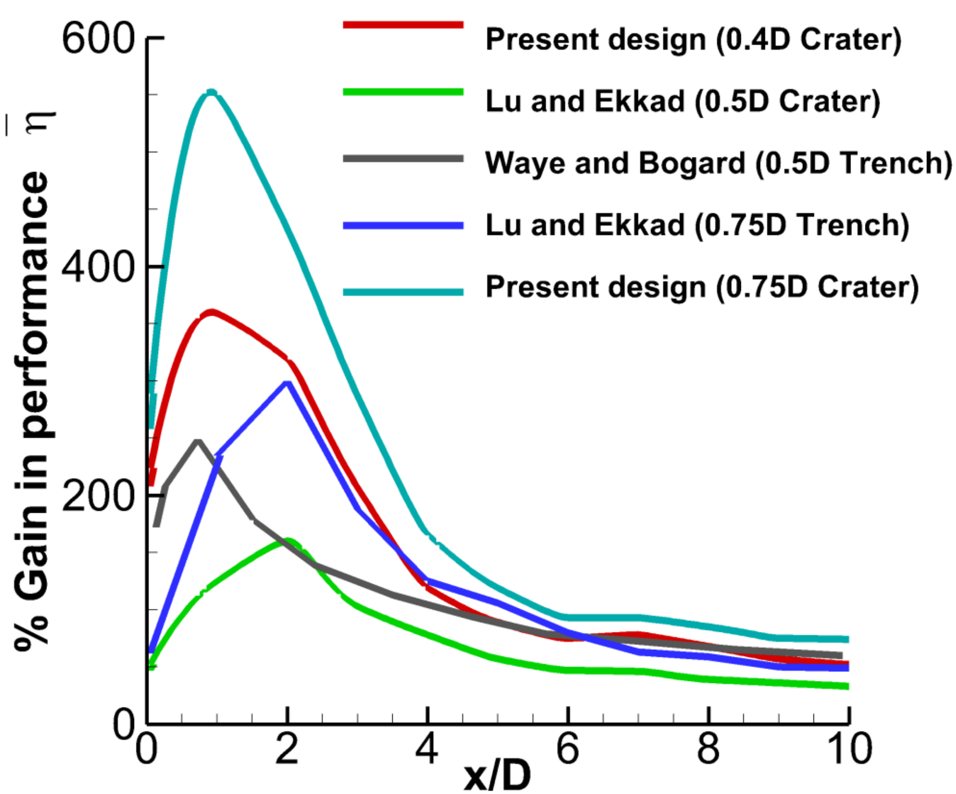

Performance at higher blowing ratios

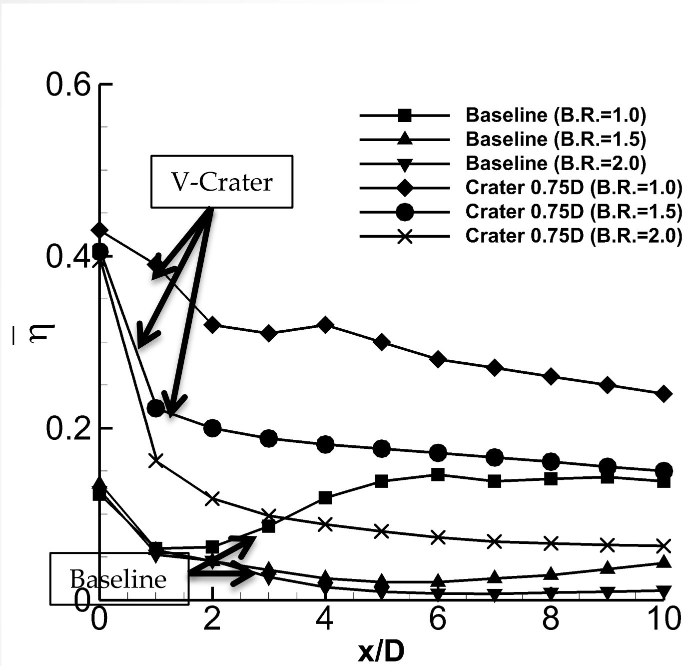

Laterally averaged film cooling effectiveness

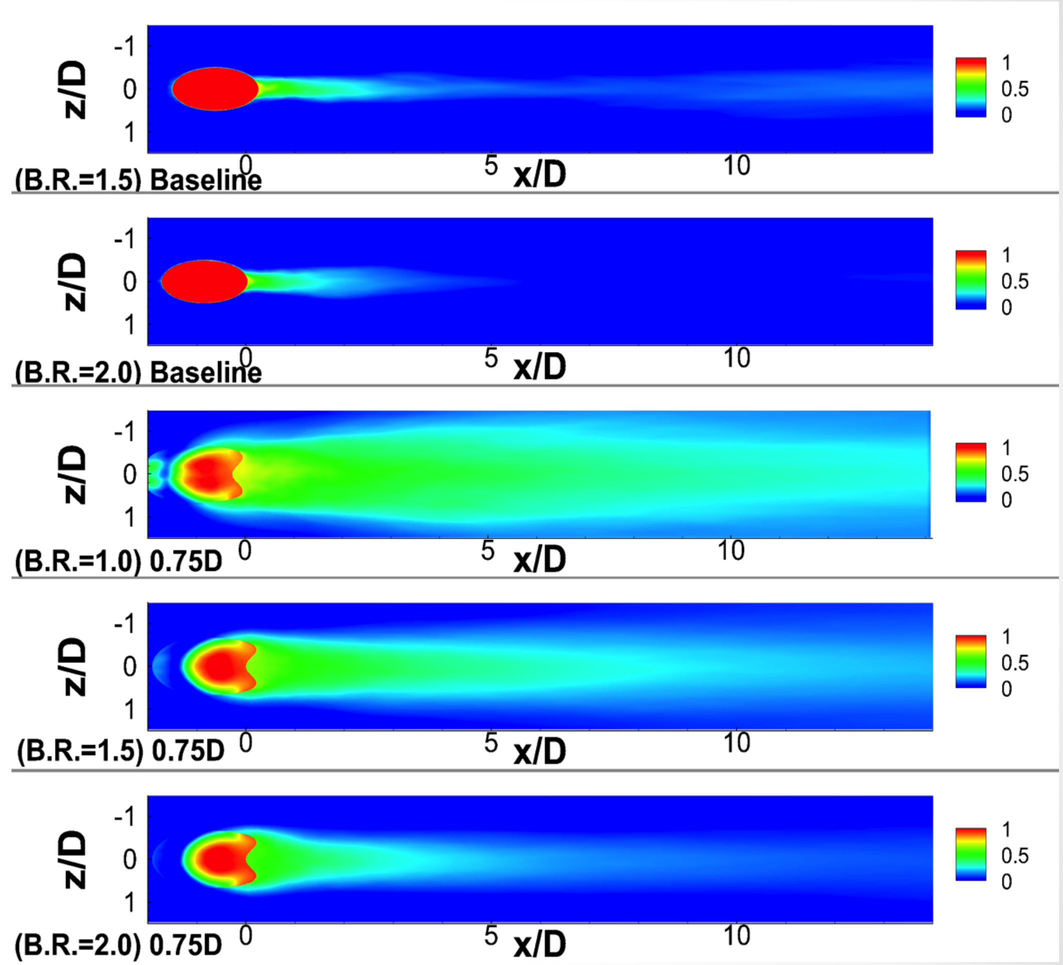

Pressure Loss

$$C_p = \frac{[(\bar{P}_0)_\infty - (\bar{P}_0)_{exit}]}{0.5\rho_\infty u_\infty^2}$$

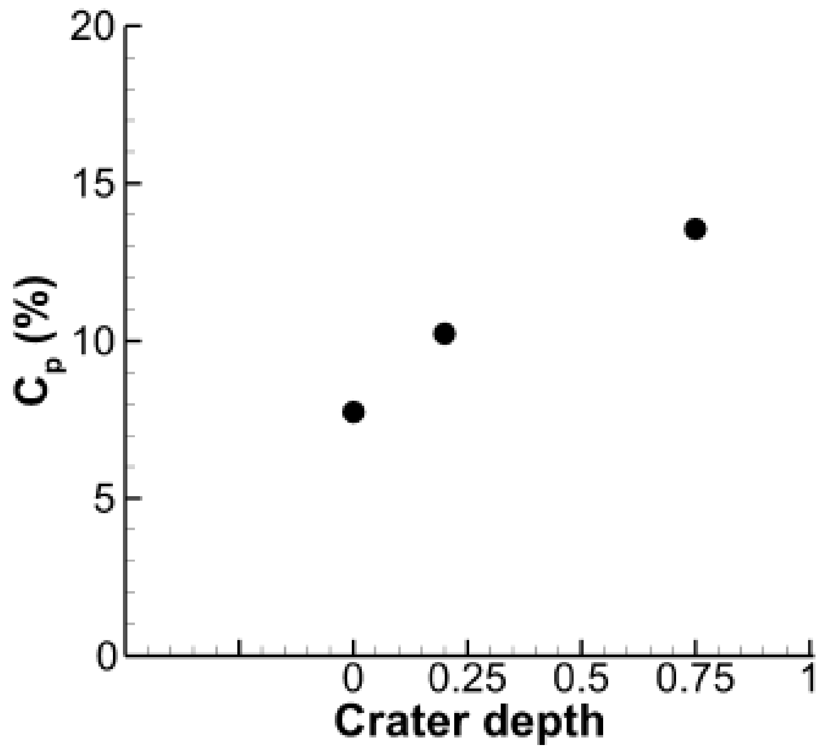

- Increases in pressure drop over baseline are observed

Outline

- Introduction
- Film Cooling Physics *(Kalghatgi & Acharya (ASME J. Turbomachinery, 2013))*
  - Coherent flow structures
  - Modal analysis
- Film Cooling Geometry (Kalghatgi & Acharya, *ASME Turbo Expo 2014)*
  - *V-cratered geometry is shown to create anti-CRVP that reduces jet-liftoff and increases surface cooling*
  - *A deeper crater (0.75D) is shown to exhibit the best cooling performance-order of 200%; associated with higher pressure drops*
  - *Baseline case shows strong spectral peaks and harmonics; the crater cases show spectral broadening and reduction of energy in the dominant modes*
- **Blowing Ratio Uncertainty Quantification** ***(Babaee, Wan & Acharya, ASME J. Heat Transfer, 2013)***
- Conclusions

The Effect of Uncertainty in Blowing Ratio on Film Cooling

- Increasing the airfoil temperature by 25°C reduces the life time of a blade by a factor of two.
- Film cooling effectiveness is strongly dependent on the blowing ratio.

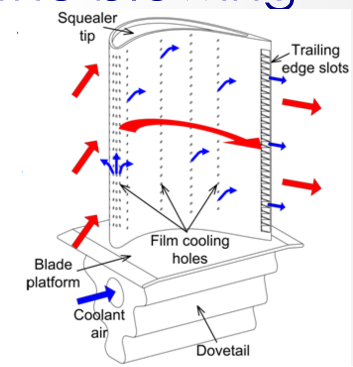

Conceptual view of blade external cooling

- In practice, the blowing ratio can vary around its designed value. This may cause the cooling effectiveness to vary potentially dropping it below the expected value used in the design.
- Need to know the effect of uncertainty or variation in the input blowing ratio on the variation in film cooling performance. Generally, the cost of computation of a traditional approach such as Monte-Carlo is the main obstacle.

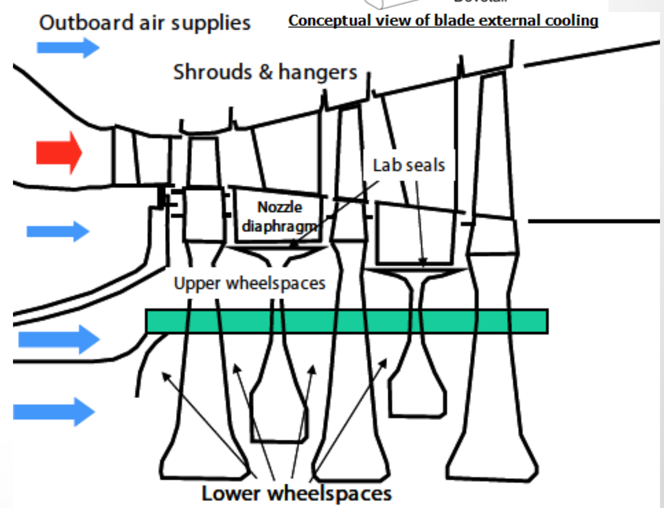

UQ Problem Specification

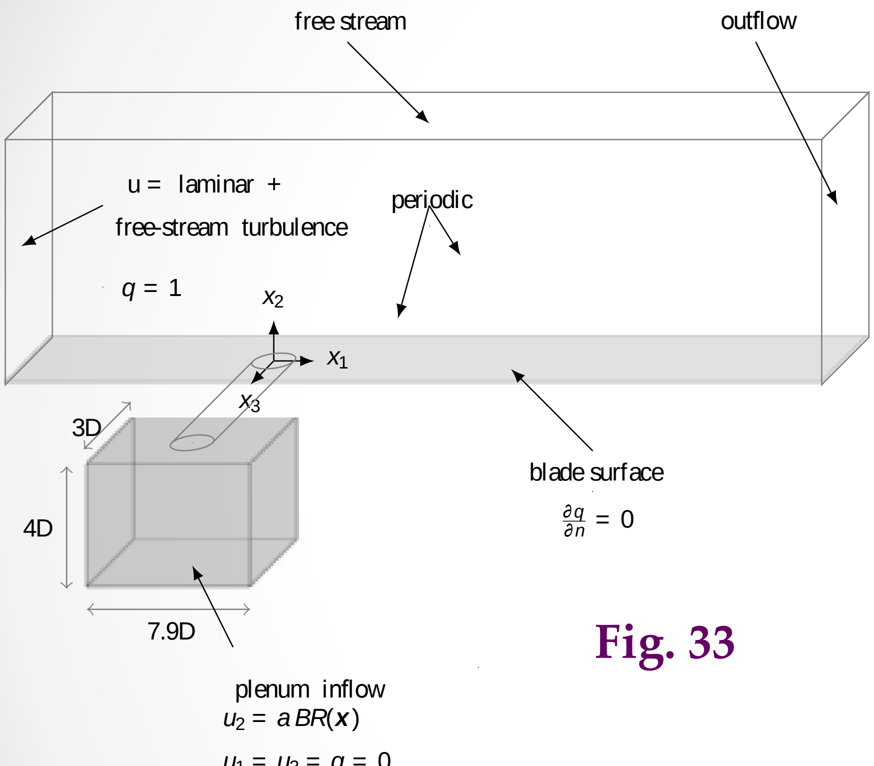

Fig. 33

- How does variation in the plenum inflow velocity (specified by a pdf) impact the surface temperature variation (what is the output pdf?)

Randomness in Blowing Ratio

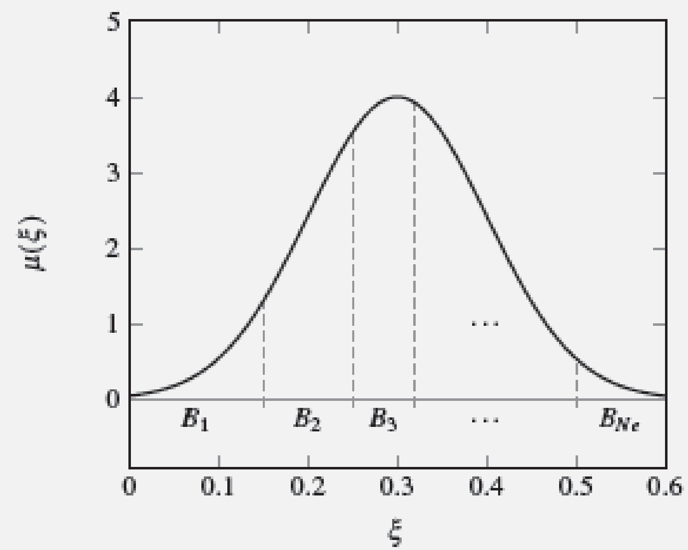

truncated Gaussian distribution

$$\mu(\xi) = \begin{cases} \mathcal{N}(m;\sigma)/\beta, & |\,\xi - m\,| \le r, \\ 0, & \text{otherwise}, \end{cases}$$

$$m = 0.3$$

$$\sigma = 0.1$$

Fig. 34

Discretization in Random Space: Multi-Element General Polynomial Chaos

- Elemental Decomposition:

$$\overline{\theta}_M(\mathbf{x};\xi) = \sum_{e=1}^{Ne}\sum_{k=0}^{M} \hat{\overline{\theta}}_k^e(\mathbf{x})\phi_k^e(\xi)$$

- Orthogonally w.r.t to the local PDF:

$$\mathbb{E}[\phi_i^e(\xi)\phi_j^e(\xi)] = (\gamma_i^e)^2\delta_{ij}$$

$$\mathbb{E}(f(\xi)) = \int_B f(\xi)\mu(\xi)d\xi$$

- Stochastic Collocation:

$$\hat{\overline{\theta}}_k^e(\boldsymbol{x}) \simeq \sum_{i=0}^{Q} w_{(i)}^e\,\theta(\boldsymbol{x};\xi_{(i)}^e)\phi_k^e(\xi_{(i)}^e)/{\gamma_k^e}^2$$

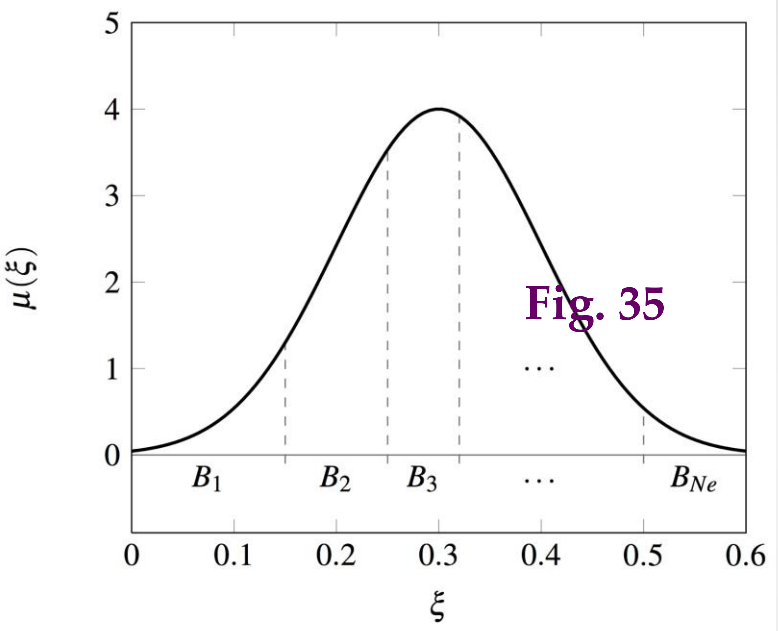

Fig. 35

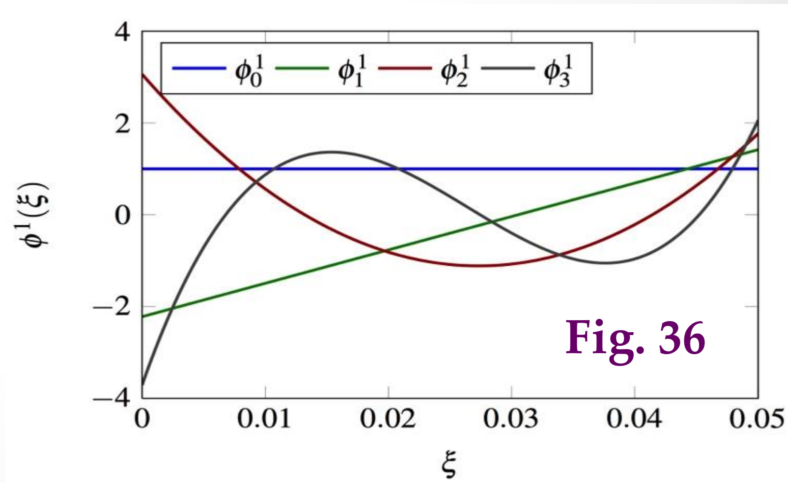

Fig. 36

Statistical Information

Offline post-processing

- Expected value:

$$\mathbb{E}[\overline{\theta}_M(\mathbf{x};\xi)] = \sum_{e=1}^{Ne}\sum_{k=0}^{M}\hat{\overline{\theta}}_k^e(\mathbf{x})\mathbb{E}[\phi_k^e(\xi)],$$

- Variance:

$$\sigma_\theta^2(\mathbf{x}) = \sum_{e=1}^{Ne}\sum_{k=0}^{M}\hat{\overline{\theta}}_k^e(\mathbf{x})^2\mathbb{E}[\phi_k^e(\xi)^2] - \sum_{e=1}^{Ne}\sum_{k=0}^{M}\hat{\overline{\theta}}_k^e(\mathbf{x})^2\mathbb{E}[\phi_k^e(\xi)]^2,$$

- Sensitivity

$$\mathcal{S}_\theta(\mathbf{x}) = \mathbb{E}\left[\frac{\partial\overline{\theta}_M(\mathbf{x};\xi)}{\partial\xi}\right] = \sum_{e=1}^{Ne}\sum_{k=0}^{M}\hat{\overline{\theta}}_k^e(\mathbf{x})\mathbb{E}[\frac{\partial\phi_k^e(\xi)}{\partial\xi}],$$

Instantaneous Temperature at Gauss Quadrature Points in Random Space

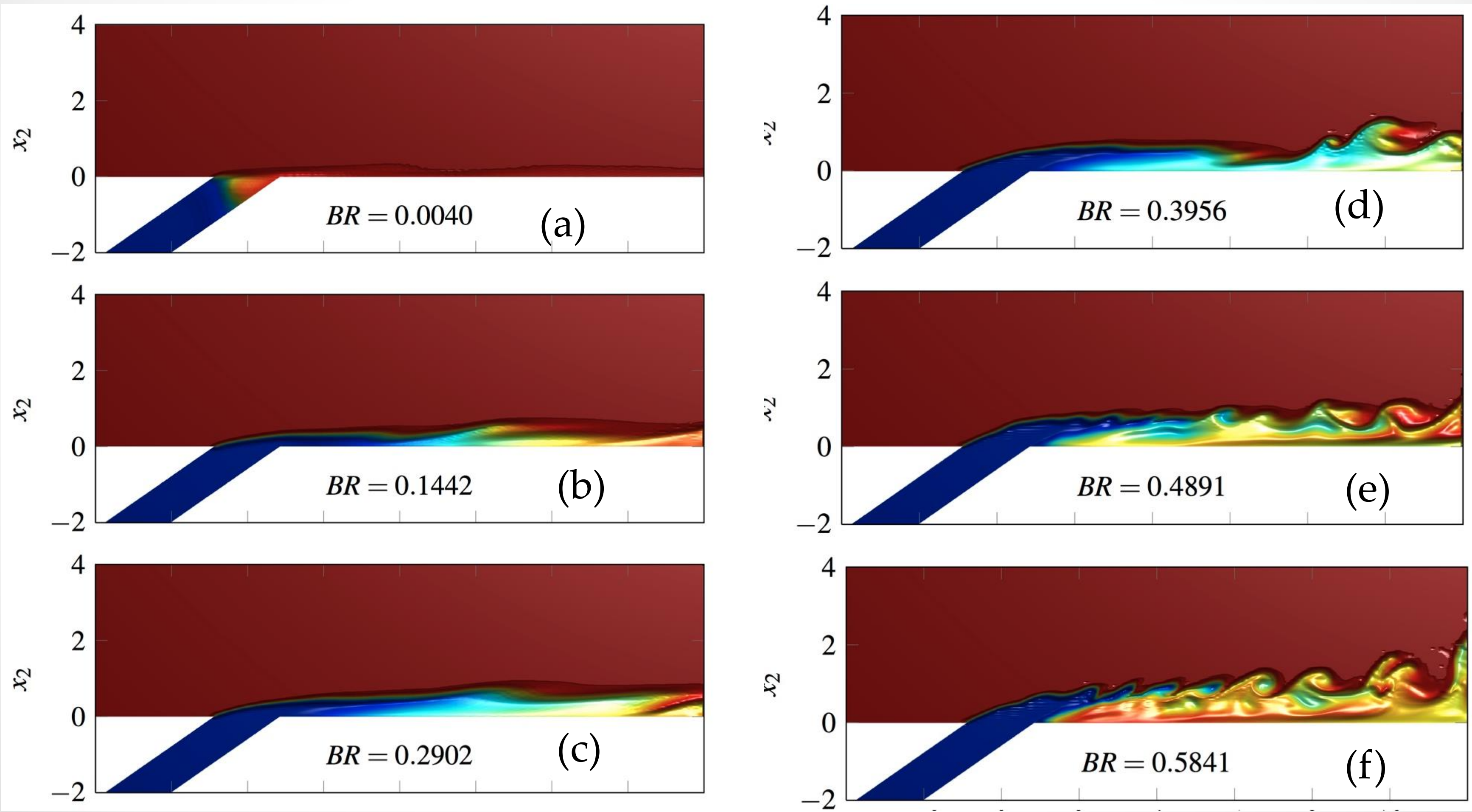

Fig. 37

Time-averaged Temperature at Gauss Quadrature Points in Random Space

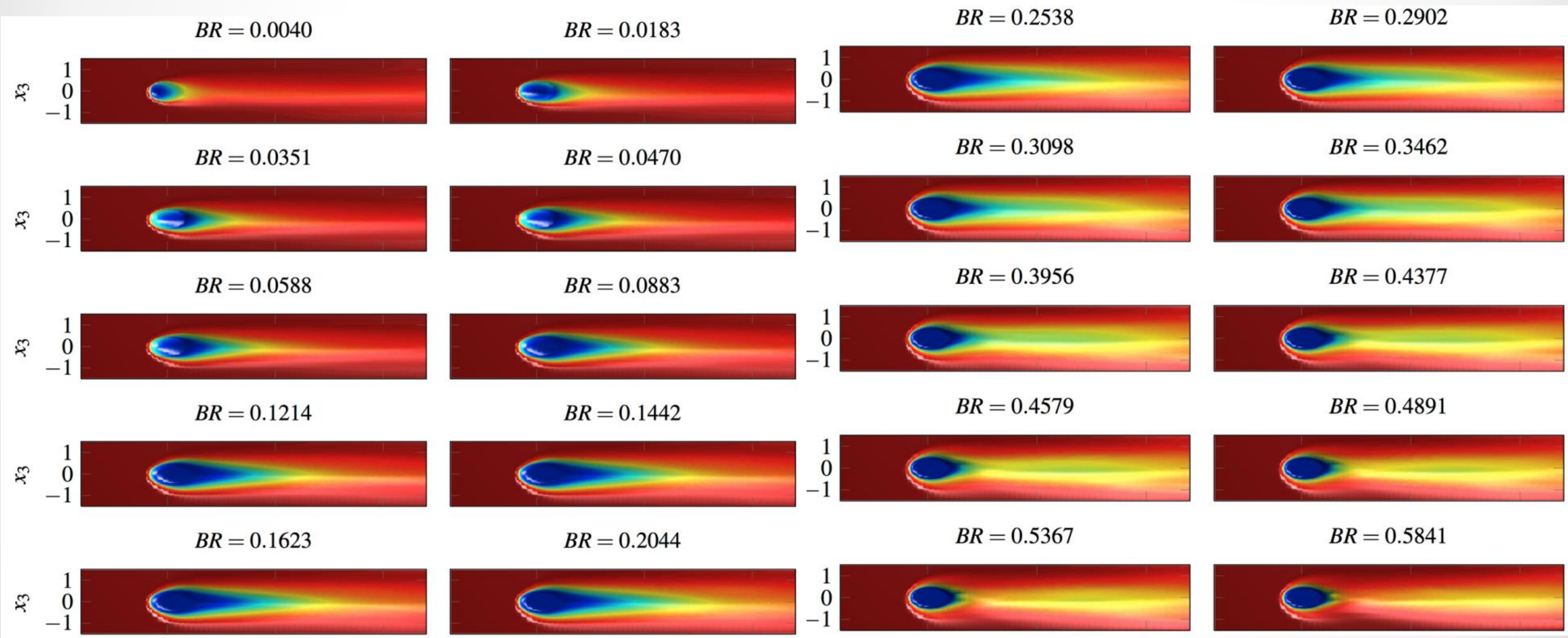

Fig. 38

Spanwise-averaged Film Cooling Effectiveness at stream-wise sections

$\mathbb{E}[\tilde{\eta}] = 0.238$ less than η of 0.25 at BR of 0.3

Variance in ñ; $\sigma_{\tilde{\eta}} = 0.022$

Cooling effectiveness range : 0.216-0.26;

Plus/minus 9.4% variation relative to expected value

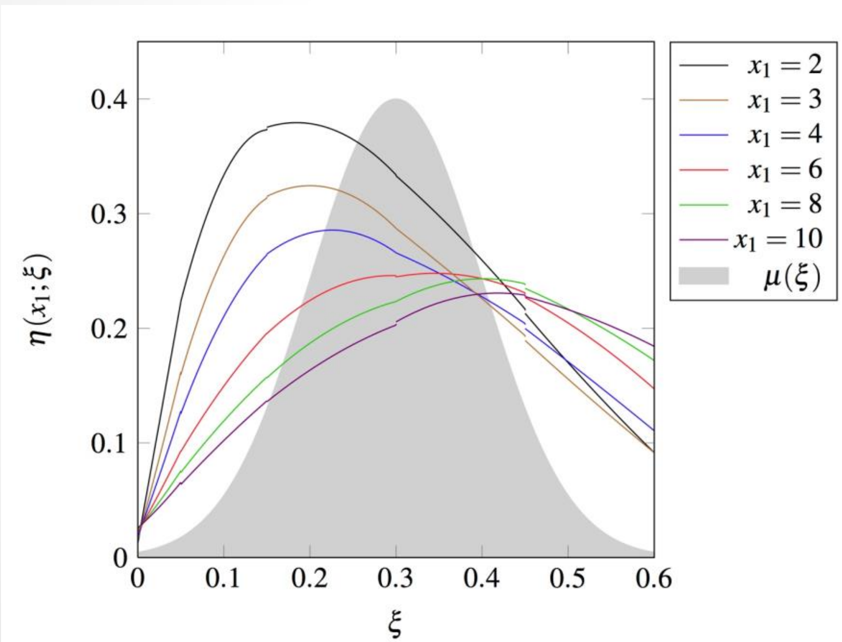

Fig. 41

$$\rho(\eta) = \mu(\xi) / \mid (d\eta/d\xi) \mid$$

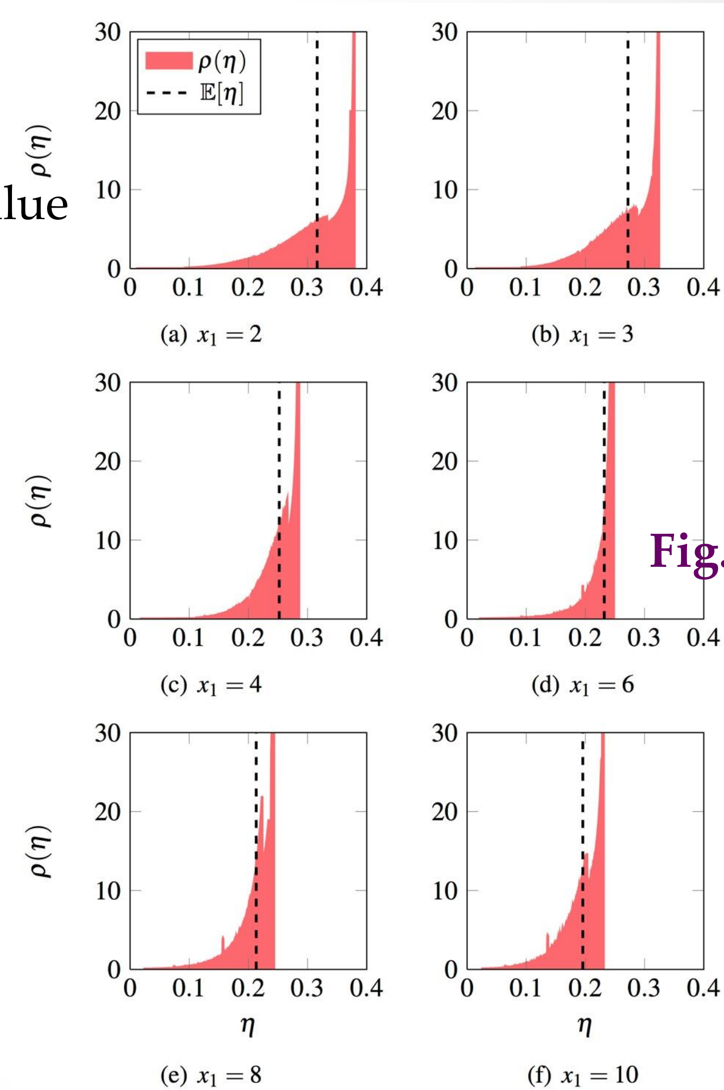

Fig. 42

Standard deviation & Optimal Point

Standard deviation of spanwise & time-averaged effectiveness

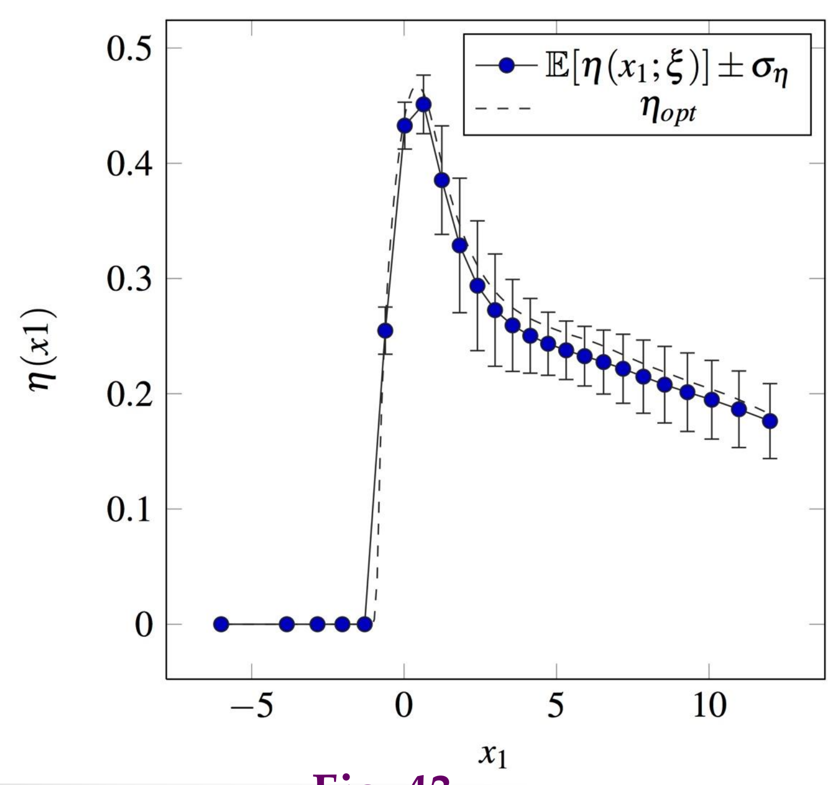

Fig. 43

Spatially-averaged film cooling effectiveness-Standard Deviation

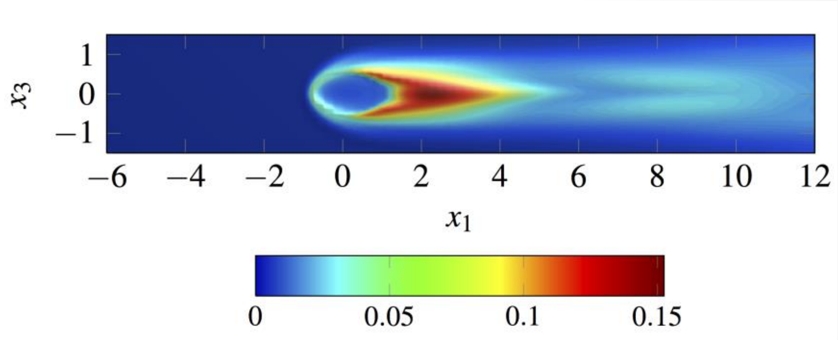

Fig. 43

Conclusion

- Modal analysis using dynamic mode decomposition.
  - Low frequency CVP modes contribute up to 18% fluctuation to film cooling effectiveness – mainly at lateral boundaries
  - K-H mode have (< 2%) on film cooling effectiveness.
- *V*-cratered geometry shown to produce significantly improved cooling effectiveness
  - Spectral broadening & lower energy is observed for the deeper craters
  - The V-shape produces anti-CRVP that reduces jet-liftoff
- UQ: The role of uncertainty in the blowing ratio on the film cooling effectiveness is explored.
  - Largest variations in effectiveness occurs within four hole diameters
  - PDF distribution of cooling effectiveness at different x location has different characteristics.